nature ecology & evolution

ARTICLES

https://doi.org/10.1038/s41559-022-01850-8

Estimating comparable distances to tipping points across mutualistic systems by scaled recovery rates

Huixin Zhang[1], Qi Wang[2], Weidong Zhang[1], Shlomo Havlin[3] and Jianxi Gao[4,5]✉

Mutualistic systems can experience abrupt and irreversible regime shifts caused by local or global stressors. Despite decades of efforts to understand ecosystem dynamics and determine whether a tipping point could occur, there are no current approaches to estimate distances (in state/parameter space) to tipping points and compare the distances across various mutualistic systems. Here we develop a general dimension-reduction approach that simultaneously compresses the natural control and state parameters of high-dimensional complex systems and introduces a scaling factor for recovery rates. Our theoretical framework places various systems with entirely different dynamical parameters, network structure and state perturbations on the same scale. More importantly, it compares distances to tipping points across different systems on the basis of data on abundance and topology. By applying the method to 54 real-world mutualistic networks, our analytical results unveil the network characteristics and system parameters that control a system's resilience. We contribute to the ongoing efforts in developing a general framework for mapping and predicting distance to tipping points of ecological and potentially other systems.

Mutualistic networks, formed when the interactions of two systems are mutually beneficial, are common in ecological[1], biological[2,3] and social systems[4,5]. Recently, mutualistic networks have attracted much attention[6–9] because their unique structural properties make them more resilient to perturbations[10,11]. However, species loss[12], invasions[13], human activities[14,15] and environmental changes[16] can cause targeted and unexpected perturbations. In a variety of real ecosystems[17–21], extensive experimental and observational evidence has shown that perturbations drive systems past tipping points and cause large-scale global extinctions[22]. Here we focus on mutualistic systems and assume the existence of tipping points as previous studies did[23–25], although we are aware that the threshold of an ecosystem is difficult to predict from empirical data[26], possibly due to noise and complicated interactions in a system[27].

Whether a particular system would collapse or could recover from a perturbation highly depends on how close the current system state is to a possible boundary[28], that is, the distance to the tipping point in a one-dimensional (1D) equation (the length of the black arrows shown in Fig. 1a). Thus, we mathematically define resilience as the distance to the boundary of the attraction basin[29]. Note that this definition is also called ecological resilience or system resilience—a system's ability to adjust its activity to retain its basic functionality when errors, failures and environmental changes occur, which is a defining property of many complex systems[30,31]. The prediction of distance to a tipping point is a grand challenge for complex systems[32,33]. There are, to our best knowledge, no theoretical approaches that can predict relative resilience among systems, considering different types of perturbations. Numerous empirical studies[17–21,34] have demonstrated how perturbations reshape the resilience of real ecosystems (Fig. 1b). Here we consider three types of perturbations: (1) structural perturbations, (2) dynamics perturbations and (3) state changes (Fig. 1b). Structural perturbations include: (1) the extinction of species (node loss) or species invasion (node addition)[35], (2) the partial removal of competitive or mutualistic interaction (link loss) or changes in weights of a few links[1] and (3) global shifts in interaction (that is, global weight loss of the entire network) caused by environmental changes such as ocean acidity or global warming[36]. Dynamics perturbations refer to changes in dynamic parameters; for example, the intrinsic growth rate α in the offspring production dynamics $dx/dt=\alpha+x(1-x)$ changes due to changes in habitat types and landscape compositions[37]. Lastly, state changes refer to changes in the initial states when solving differential equations. They include patterns of temporal variation altered by a sharp drop in species abundance after, for example, a tsunami[38], and the recovery of an ecosystem such as the coastal ecosystem through the restoration of seagrass habitat in the Chesapeake Bay in the USA[39]. Numerous empirical studies[17–21,34] have demonstrated how these different types of perturbations simultaneously reshape the resilience of real ecosystems. They can happen simultaneously and add compounding effects on ecological networks and thus, push them across their tipping point in diverse ways, bringing profound challenges to predicting the distances to their tipping points.

Many research efforts attempt to monitor system-level behaviour when a network is approaching its tipping point[40] (Fig. 1c) in the hope of preventing the system from collapsing into undesired states[41]. These efforts greatly fructify the development of metrics, like recovery rate (that is, speed of recovery from perturbation) and autocorrelation variance (self-similarity near a tipping point)[23,42,43]. However, none of these metrics can explicitly measure distances to tipping points, let alone compare them across different systems. Comparing two snapshots can at best inform us whether a given system is moving towards its tipping point (for example, (i) and (ii) in Fig. 1c), providing no information in the units of changes in the parameter driving a system to its tipping point. Also, one system can react differently when facing different perturbations (for example,

[1]Department of Automation, Shanghai Jiao Tong University, Shanghai, China. [2]Department of Civil and Environmental Engineering, Northeastern University, Boston, MA, USA. [3]Department of Physics, Bar-Ilan University, Ramat-Gan, Israel. [4]Department of Computer Science, Rensselaer Polytechnic Institute, Troy, NY, USA. [5] Network Science and Technology Center, Rensselaer Polytechnic Institute, Troy, NY, USA. ✉e-mail: jianxi.gao@gmail.com

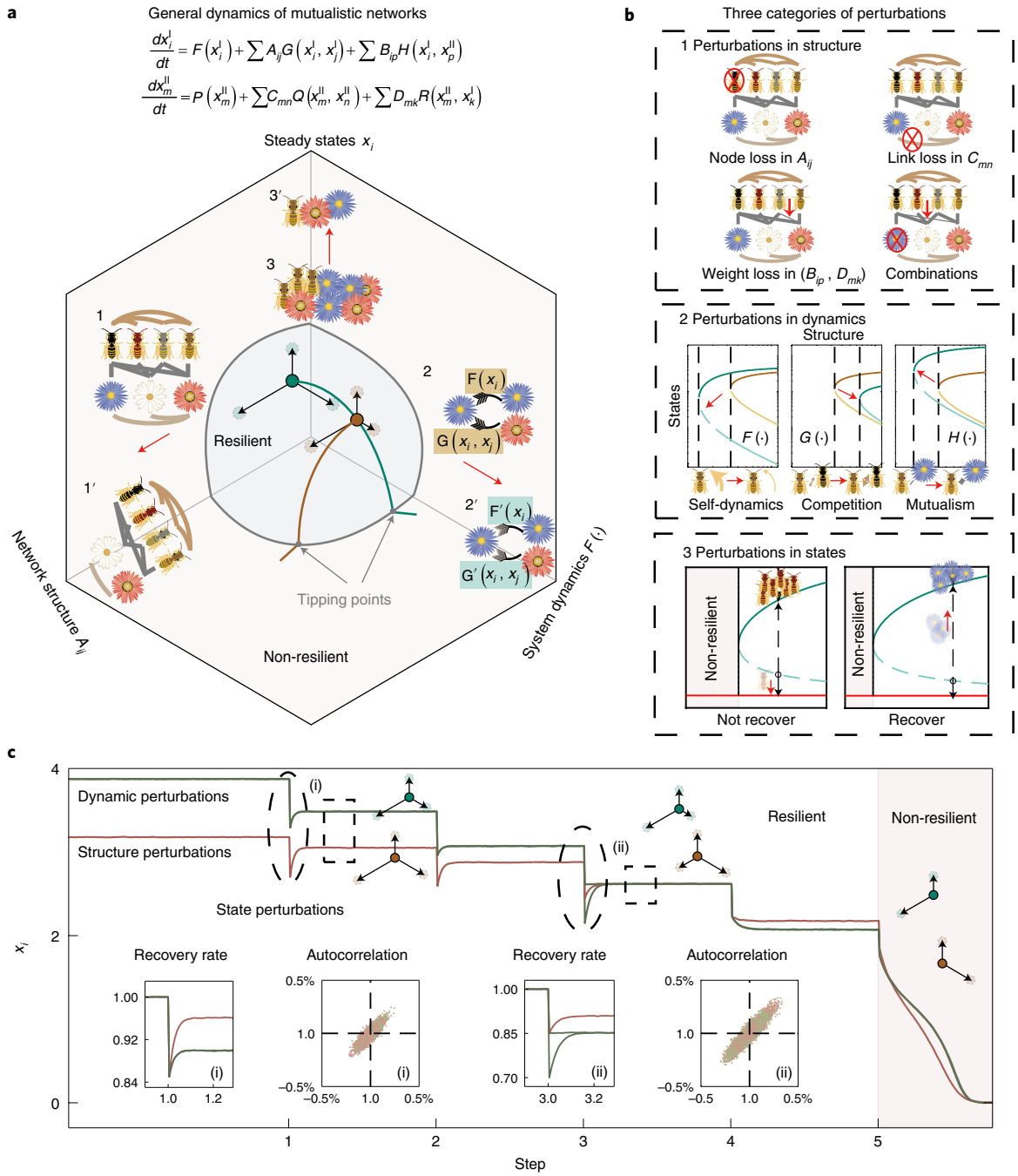

Fig. 1 | Early-warning signals indicate distance to tipping points of mutualistic networks. a, A common approximation of the behaviour of mutualistic networks is high-dimensional interacting equations, capturing both dynamical roles (tailed arrows, including: self-dynamics, $F(\cdot)$ and $P(\cdot)$; competitive-dynamics, $G(\cdot)$ and $Q(\cdot)$; mutualistic-dynamics, $H(\cdot)$ and $R(\cdot)$) and structural properties (including: interactions within one system, A_{ij} and C_{ij}; interactions between two systems, B_{ij} and D_{ij}). How one system behaves after one perturbation (the red arrow) is predominantly determined by network structure (the brown curve), system dynamics (the green curve) and its current state. Whether this mutualistic network could collapse (non-resilient) or recover (resilient) from a perturbation highly depends on how close the current resilience of this system is to the edge (the grey curves), that is, the distance to the tipping point (black arrows). **b**, Perturbations that challenge the resilience of one system can be classified as: (1) perturbations in structure, (2) perturbations in dynamics (from one dynamic role, marked as brown, to another dynamic role, marked as green; the solid curve represents the stable state, while the dashed curve represents the unstable state) and (3) perturbations in the current state, which leading to (the black arrow) the resilient state or the non-resilient state (the red curve). **c**, We simulated how a 1D equation $\frac{dx}{dt} = x(\alpha - \beta x + \frac{\gamma x}{1+h\gamma x})$ ($\beta = 1, h = 0.2$) behaves after perturbations (occur at steps 1, 2, 3, 4 and 5), including dynamic perturbation (green curve, $\gamma = [8: -1: 3]$), structure perturbation (brown curve, $\alpha = -[0.1: 0.3: 1.6]$) and state perturbation (dashed circle, $x_0 = x_s[0.85, 0.7]$). As the distance to a tipping point shortens (i vs ii), recovery rate becomes slower and autocorrelation (detected during the stable period, marked as dashed rectangles) becomes larger. However, two systems that have the same metrics may be unequally resilient (brown curve in (i) vs green curve in (ii)).

the two green curves for the same location (ii) in Fig. 1c). Moreover, two systems can have the same values in these metrics but vary in their distances to tipping points. The difference is due to each system being governed by a unique set of high-dimensional dynamical equations with different network structures[7]. As shown in Fig. 1c, a system can have similar recovery rates at step 1 (that is, green curve (i)) and step 3 (that is, brown curve (ii)). The fact that recovery rates are a general way of assessing a system's resilience and that they can be quantified in a broad range of systems, regardless of their specific characteristics, hints at its broad applicability and calls for the development of a more general framework.

Here we develop a novel mathematical framework to position various systems with different dynamical parameters, network structures and state variables on the same scale, making it possible to directly compare their distances to tipping points. This framework provides: (1) a structural indicator that measures the resilience of a system and (2) a scaling factor that positions the resilience of different systems on the same scale. It allows us to measure distances to tipping points across mutualistic systems with critical thresholds and thus quantify their resilience on the same scale using data on abundance and topology (see Extended Data Fig. 1).

Results

To obtain a general framework for mutualistic networks, we first introduce a well-studied model from the literature which assumes nonlinear dynamics. Here we use the same set of differential equations as in ref. [44], which considers mutualistic interactions between plants and animals (for example, plants and their pollinators), as well as interspecific competitions within plants and animals. The model incorporates complex and critical elements—such as saturated functional responses[45] and interspecific competition within a guild[7]—recently adduced as essential components of mutualistic interactions. Specifically, the dynamical model has the following form:

$$\begin{aligned}\frac{dP_i}{dt} &= P_i\left[\alpha_i^{(P)} - \sum \beta_{ij}^{(P)} P_j + \frac{\sum \gamma_{ik}^{(P)} A_k}{1+h_i^{(P)} \sum \gamma_{ik}^{(P)} A_k}\right]\\ \frac{dA_i}{dt} &= A_i\left[\alpha_i^{(A)} - \sum \beta_{ij}^{(A)} A_j + \frac{\sum \gamma_{ik}^{(A)} P_k}{1+h_i^{(A)} \sum \gamma_{ik}^{(A)} P_k}\right]\end{aligned}, \quad (1)$$

where (P) and (A) stand for plant and animal, respectively. P_i and A_i are their abundances. α_i denotes species i's intrinsic growth rate in the absence of competition and mutualism, β_{ij} captures the direct interspecific competition of resources between species i and j, h_i is the saturating constant of the beneficial effect of mutualism[7,44] and γ_{ij} defines the per capita mutualistic strength between one plant and one animal. The last term of equation (1) describes the mutualistic interaction through nonlinear functional responses representing a saturation of consumers as the resources increase.

The dimension reduction on mutualistic networks. The high dimensionality in mutualistic networks, brought about by the complex interactions of competitive and mutualistic effects, determines the high dimensionality in the basin attractions. In this way, the distance to the boundary of the attraction basin (a surface) is in all directions, and thus, it is intractable to calculate how far the system is to losing its resilience. The difficulty is rooted in the interaction terms, such as $\sum \beta_{ik}$ and $\sum \gamma_{ik}$, where the matrices (for example, γ_{ik} for mutualism and β_{ik} for competition) link all the nonlinear equations coupled together. Without loss of generality, we use a matrix M to represent all possible interactions discussed in this work, such as competitive interactions (matrix $\beta^{(A)}$ for animals and matrix $\beta^{(P)}$ for plants) and mutualistic relations (matrix $\gamma^{(P)}$ and $\gamma^{(A)}$ for the mutualism between the two systems). Here we focus on quantities related to the average nearest-neighbour node. Consider a scalar quantity y_i related to node i, for example, i's activity $x_i(t)$ at time t. The mean value of y_i over all nodes is given by $\langle y_i\rangle = 1/N\sum_{i=1}^{N} y_i$. This is different, however, from the mean over all nearest-neighbour nodes, $\langle y_i\rangle_{\mathrm{nn}}$. Indeed, when sampling nearest-neighbour nodes, our selection process is biased towards the more connected nodes, as nodes with many nearest neighbours are sampled more often[46]. We thus construct the following averaging procedure: for each node i, a neighbour j is selected with probability proportional to j's outgoing link M_{ij}. With this selection procedure, nodes with a greater outgoing degree $s_j^{\mathrm{out}} = \sum_{i=1}^{N} M_{ij}$ are more likely to be selected, and as a result their weight in the construction of $\langle y_i\rangle_{\mathrm{nn}}$ is proportional to s_j^{out}. Thus, we compress a sum over all of i's nearest neighbours j as $s_i^{\mathrm{in}}\langle y_j\rangle_{\mathrm{nn}}$, where $s_i^{\mathrm{in}} = \sum_{j=1}^{N} A_{ij}$. For networks with little degree correlations, we take the average over j to be independent of i, that is, we assume that i's neighbourhood is, on average, identical to the neighbourhood of all other nodes. This allows us to write average state as $s_i^{\mathrm{in}}\langle y_j\rangle_{\mathrm{nn}}$, without specifically attributing the average to nearest neighbours of i. To formalize the above analysis, we introduce the operator

$$y = \mathcal{L}(M, \mathbf{y}) = \frac{1^{\top} M \mathbf{y}}{1^{\mathrm{T}} M 1}, \quad (2)$$

where $1 = (1, \ldots, 1)^{\mathrm{T}}$ is the unit vector. This operation, equation (2), enables us to compress the high-dimension information y into a scalar y. The input vector $\mathbf{y}$ can be the element's states (P_i and A_i), the dynamical parameters (α_i) and the structural properties (weighted degrees s).

Since a mutualistic system has four network structures, as the four inputs of the mean-field operator (equation (2)), we can condense the governing high-dimension dynamics (equation (1)) into a four-dimensional function

$$\begin{aligned}\frac{dP^{\mathrm{P}}}{dt} &= P^{\mathrm{P}}\left(\alpha^{\mathrm{PP}} + \beta_s^{\mathrm{PP}} P^{\mathrm{P}} + \beta^{\mathrm{PP}} P^{\mathrm{P}} + \frac{\gamma^{\mathrm{PP}} A^{\mathrm{P}}}{1+h^{\mathrm{PP}}\gamma^{\mathrm{PP}} A^{\mathrm{P}}}\right)\\ \frac{dA^{\mathrm{A}}}{dt} &= A^{\mathrm{A}}\left(\alpha^{\mathrm{AA}} + \beta_s^{\mathrm{AA}} A^{\mathrm{A}} + \beta^{\mathrm{AA}} A^{\mathrm{A}} + \frac{\gamma^{\mathrm{AA}} P^{\mathrm{A}}}{1+h^{\mathrm{AA}}\gamma^{\mathrm{AA}} P^{\mathrm{A}}}\right)\\ \frac{dP^{\mathrm{A}}}{dt} &= P^{\mathrm{A}}\left(\alpha^{\mathrm{PA}} + \beta_s^{\mathrm{PA}} P^{\mathrm{A}} + \beta^{\mathrm{PA}} P^{\mathrm{P}} + \frac{\gamma^{\mathrm{PA}} A^{\mathrm{P}}}{1+h^{\mathrm{PA}}\gamma^{\mathrm{PA}} A^{\mathrm{P}}}\right)\\ \frac{dA^{\mathrm{P}}}{dt} &= A^{\mathrm{P}}\left(\alpha^{\mathrm{AP}} + \beta_s^{\mathrm{AP}} A^{\mathrm{P}} + \beta^{\mathrm{AP}} A^{\mathrm{A}} + \frac{\gamma^{\mathrm{AP}} P^{\mathrm{A}}}{1+h^{\mathrm{AP}}\gamma^{\mathrm{AP}} P^{\mathrm{A}}}\right)\end{aligned}. \quad (3)$$

Here, PP reflects the average information of plants from the perspective of plants themselves, while PA reflects evaluation from the perspective of animals (more details can be found in Table 1). The advance of our current study from the previous approaches[31,47] lies on the ability to: (1) deal with multilayer networks[48], whereas the previous focus is on single networks; (2) map a bipartite network with a rectangular matrix ($N^{\mathrm{I}} \times N^{\mathrm{II}}$) to a single number, whereas the previous method can only treat a square matrix of a unipartite network.

Furthermore, we reconstruct the low-dimensional information obtained above as an adjacency matrix $Z = [\beta^{\mathrm{PP}} 0 0 \gamma^{\mathrm{PP}}; 0 \beta^{\mathrm{AA}} \gamma^{\mathrm{AA}} 0; \beta^{\mathrm{PA}} 0 0 \gamma^{\mathrm{PA}}; 0 \beta^{\mathrm{AP}} \gamma^{\mathrm{AP}} 0]$. Then we further compress the four-dimensional function (equation (3)) into a one-dimensional function by putting matrix Z as the input matrix of operator $\mathcal{L}(Z, \mathbf{y})$ and finally get

$$\frac{dx}{dt} = x\left[\alpha - (\beta_s + \beta)\, x + \frac{\gamma x}{1 + h\gamma x}\right] = \Delta f(\alpha, \beta_w, \gamma, x), \quad (4)$$

where $\beta_w = \beta + \beta_s$, x captures the mean-field abundance of both plants and animals (more details in Table 2). The system (equation (4)) characterizes the one-dimensional abundance x of both plants, P_i, and animals, A_i. The transformation provides a general one-dimensional function to study the resilience of mutualistic networks and apply traditional tools designed for one-dimensional

Table 1 | Effective variables abstracted from adjacency matrices. Effective variables obtained from the operator $\mathcal{L}(M, \mathbf{y})$, with the input matrix M as competitive structure ($\beta^{(P)}$, $\beta^{(A)}$) and mutualistic structure ($\gamma^{(P)}$, $\gamma^{(A)}$), and the input vector y as states (P_i, A_i), growth rates (α_i), self-competition strength (β_{si}) and the number of i's interactions (s_i). We set that the saturating constant h_i is homogeneous for all species and thus we have $h^{PP} = h^{AA} = h^{PA} = h^{AP} = h$

	M	y	Description
P^P	$\beta^{(P)}$	(P_i)	Effective abundance of plants, considering contributions from plants
A^A	$\beta^{(A)}$	(A_i)	Effective abundance of animals, considering contributions from animals
P^A	$\gamma^{(A)}$	(P_i)	Effective abundance of plants, considering contributions from animals
A^P	$\gamma^{(P)}$	(A_i)	Effective abundance of animals, considering contributions from plants
α^{PP}	$\beta^{(P)}$	$\alpha^{(P)}$	Effective growth rate of plants, considering contributions from plants
α^{AA}	$\beta^{(A)}$	$\alpha^{(A)}$	Effective growth rate of animals, considering contributions from animals
α^{PA}	$\gamma^{(A)}$	$\alpha^{(P)}$	Effective growth rate of plants, considering contributions from animals
α^{AP}	$\gamma^{(P)}$	$\alpha^{(A)}$	Effective growth rate of animals, considering contributions from plants
β_s^{PP}	$\beta^{(P)}$	$\beta_s^{(P)}$	Effective self-competition of plants, considering contributions from plants
β_s^{AA}	$\beta^{(A)}$	$\beta_s^{(A)}$	Effective self-competition of animals, considering contributions from animals
β_s^{PA}	$\gamma^{(A)}$	$\beta_s^{(P)}$	Effective self-competition of plants, considering contributions from animals
β_s^{AP}	$\gamma^{(P)}$	$\beta_s^{(A)}$	Effective self-competition of animals, considering contributions from plants
β^{PP}	$\beta^{(P)}$	$\mathbf{s}^{I}$	Effective competition of plants, considering contributions from plants
β^{AA}	$\beta^{(A)}$	$\mathbf{s}^{II}$	Effective competition of animals, considering contributions from animals
β^{PA}	$\gamma^{(A)}$	$\mathbf{s}^{I}$	Effective competition of plants, considering contributions from animals
β^{AP}	$\gamma^{(P)}$	$\mathbf{s}^{II}$	Effective competition of animals, considering contributions from plants
γ^{PP}	$\gamma^{(P)}$	$\mathbf{s}^{Ic}$	Effective mutual strength of plants, considering contributions from plants
γ^{AA}	$\gamma^{(A)}$	$\mathbf{s}^{IIc}$	Effective mutual strength of animals, considering contributions from animals
γ^{PA}	$\gamma^{(A)}$	$\mathbf{s}^{Ic}$	Effective mutual strength of plants, considering contributions from animals
γ^{AP}	$\gamma^{(P)}$	$\mathbf{s}^{IIc}$	Effective mutual strength of animals, considering contributions from plants

Table 2 | Effective variables abstracted from the effective matrix Z. Effective variables obtained from the operator $\mathcal{L}(M, \mathbf{y})$, with the input matrix M as reconstructed matrix Z, and the input vector y as effective states ($[P^P, A^A, P^A, A^P]^T$), effective growth rates ($[\alpha^{PP}, \alpha^{AA}, \alpha^{PA}, \alpha^{AP}]^T$), effective self-competition strength ($[\beta_s^{PP}, \beta_s^{AA}, \beta_s^{PA}, \beta_s^{AP}]^T$), effective competitive strength ($[\beta^{PP}, \beta^{AA}, \beta^{PA}, \beta^{AP}]^T$) and effective mutualistic strength ($[\gamma^{PP}, \gamma^{AA}, \gamma^{PA}, \gamma^{AP}]^T$)

	M	y	Description
x	Z	$[P^P, A^A, P^A, A^P]^T$	Effective abundance for both plants and animals
α	Z	$[\alpha^{PP}, \alpha^{AA}, \alpha^{PA}, \alpha^{AP}]^T$	Effective growth rate for both plants and animals
β_s	Z	$[\beta_s^{PP}, \beta_s^{AA}, \beta_s^{PA}, \beta_s^{AP}]^T$	Effective self-competition for both plants and animals
β	Z	$[\beta^{PP}, \beta^{AA}, \beta^{PA}, \beta^{AP}]^T$	Effective competition for both plants and animals
γ	Z	$[\gamma^{PP}, \gamma^{AA}, \gamma^{PA}, \gamma^{AP}]^T$	Effective self-competition for both plants and animals

systems with small parameter space[49]. After the transformation into the one dimension, the state of a high-dimensional system could be easily positioned in a line, corresponding to the resilient region (above the tipping point, non-zero biomass, $x>0$ in equation (1)) or the non-resilient region (below the tipping point, zero biomass, $x=0$ in equation (1)).

The developed one-dimensional function, that is, equation (4), can predict the dynamical behaviours of mutualistic networks regardless of the types of perturbations. As illustrated in Fig. 1b, mutualistic networks can face various perturbations. Each can lead to complex behaviours depending on the system's size, structure and consequentially, its boundaries of operating space[8,50,51]. We examine such complexity by imposing simulated perturbations on 39 pollinator networks worldwide (Supplementary Table 1). The perturbations are applied on links (reducing/increasing their strength on average by a fraction f_w, removing/adding a fraction, f_l, of links randomly) and nodes (removing a fraction of plants f_{pN} or eliminating a fraction of animals f_{aN}). We simulate the dynamics of species using equation (1), providing the average abundance of all plants ($\langle P\rangle$) and that of animals ($\langle A\rangle$) across 100 realizations. The realization results for one network with $\alpha=-0.3$, $\beta_s=3$, $h=0.2$, are shown in Fig. 2a–p (see complete results for all 39 networks in Supplementary Figs. 8–15 and prediction errors in Supplementary Table 5). After applying the reduction, the numerical results (red points in Fig. 2q) collapse onto the resilience plane (blue surface in Fig. 2q) predicted by our approach (equation (4)). The convergence indicates that our mutualistic function predicts the behaviours of dynamics of ecological networks regardless of the types of perturbation.

The resilience phase space of mutualistic networks. With the one-dimensional resilience function (equation (4)), we can measure the resilience of a high-dimensional system with a simple variable x, which denotes the weighted average biomass of all species using our reduction approach.

Our framework decouples the intertwined competition and mutualism in the same one-dimensional function. Thus, the analysis focusing on a one-dimensional resilience function can elucidate the dynamic roles of competition and mutualism in a mutualistic system. In a one-dimensional system (for example, $\alpha=-1$, $\beta_s=4$, $h=0.2$ in Fig. 3) with fixed competitive interaction ($\beta=0.2$ in Fig. 3a,b), the mutualistic interaction γ alone determines the state of the system. When the mutual strength γ is less than its critical value γ_c (see Supplementary Note 2 for the derived process), that is, $\gamma<\gamma_c$, the system (equation (4)) will undergo a single first-order transition from high biomass ($x>0$) to low biomass ($x=0$). By setting $f(\alpha,\beta_s,\beta,\gamma,x)=\alpha-(\beta_s+\beta)x+\frac{\gamma x}{1+h\gamma x}$, we get that if γ is smaller than $\gamma_c^1=(\beta_s+\beta)\frac{(1-h\alpha)+2\sqrt{-h\alpha}}{(1+h\alpha)^2}$, $f(\alpha,\beta_s,\beta,\gamma)$ is always smaller than 0 (with the strength $\beta_s\geq 0$, $\beta\geq 0$, $\gamma\geq 0$) and all species eventually become extinct due to the lack of mutualism. In this scenario, 0 is the only fixed point in equation (4).

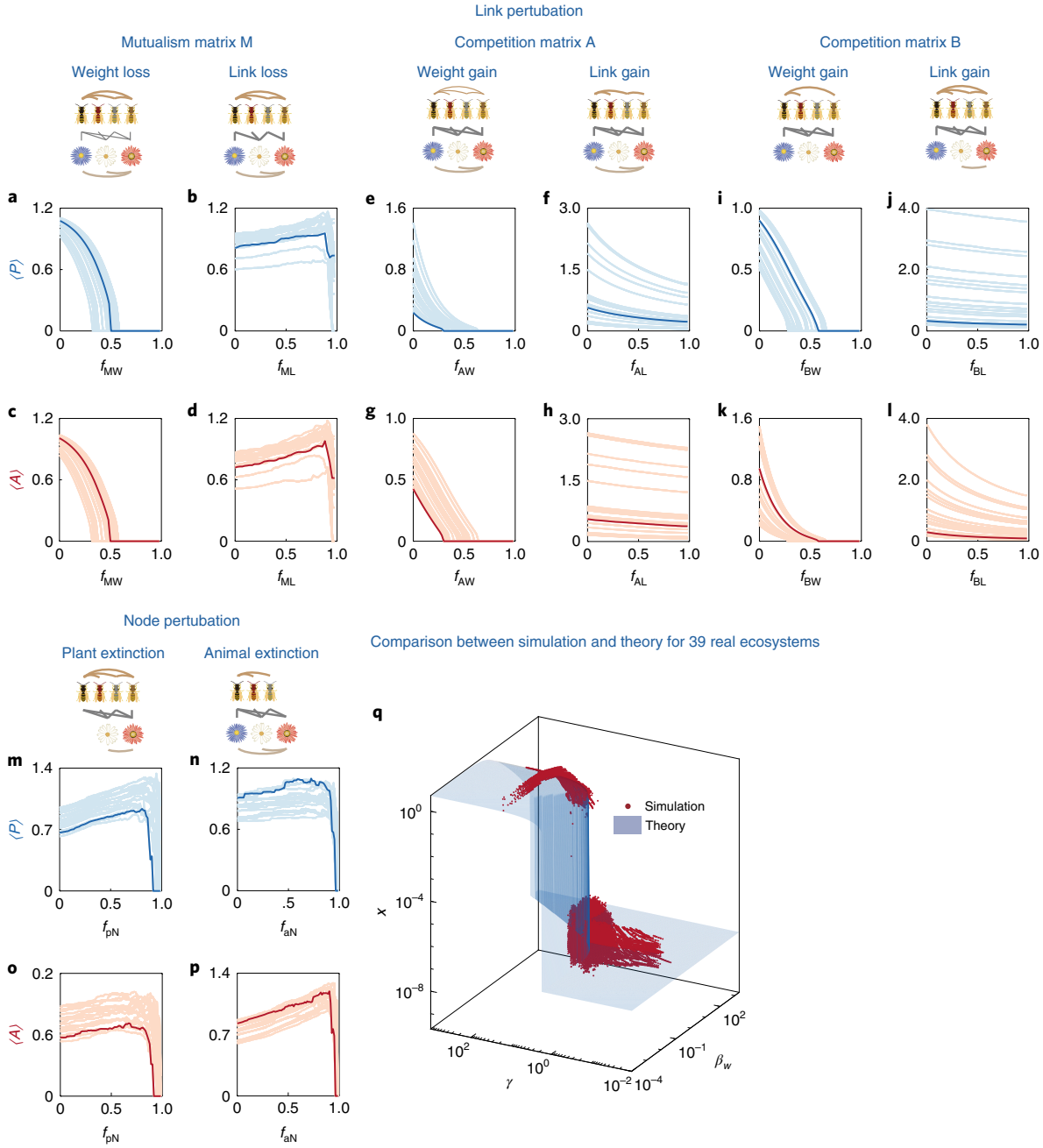

Fig. 2 | The resilience function of mutualistic networks to structural perturbations. a–p, We tested the resilience of the system (equation (1), $\alpha_i=\alpha=-0.3$, $\beta_{si}=\beta_s=3$, $h_i=h=0.2$) with both competition (links random, $\beta_{ij}=0.03$ with probability 50%) and mutualism. The network data are from ref. [66] as shown in Supplementary Table 1, $\gamma_{ij}=\frac{\gamma_0}{\langle s_i\rangle t}$ with $\gamma_0=9$ and $t=0.2$. Their resilience is tested against: (1) perturbation in links (**a–l**); and (2) perturbation in nodes (**m–p**). Link perturbation has two variations: increasing/decreasing (that is, competition/mutualism) the average weight to a fraction f_w of their original value; and extinction of a fraction f_L of links. Node perturbation also has two variations: extinction of a fraction f_{pN} of plants; extinction of a fraction f_{aN} of animals. **q**, All data (red points, simulation) in **a–p** and in Supplementary Figs. 8–15, comprising 39 highly diverse empirical ecological networks. They uniformly collapse onto the resilience function (blue surface, theory, 1D equation (4)), indicating that regardless of the network structure and the form of perturbation, the state of the system is captured by β and γ (see prediction error in Extended Data Fig. 2).

Additionally, we introduce γ_c^2, which describes the minimal strength of mutualistic interaction that leads the system from its initial state (x_0) to the fixed point $x>0$, with the expression $\gamma_c^2=\frac{1}{hx_0}[\frac{1}{h\alpha-h(\beta_s+\beta)x_0+1}-1]$. The system cannot maintain its resilient state (the stable state with high biomass, blue line in Fig. 3a) if $\gamma<\gamma_c^1=13.74$, and with low initial x_0 (for example, $x_0=0.01$), it will lose its resilience if $\gamma<\gamma_c^2=131.67$. Intriguingly, the existence of γ_c^2 depends on both the initial state x_0 and the competition strength β (Fig. 3b). The competition strength β also influences γ_c^1, that is, $\gamma_c^1=f(\beta)$, and thus we can write γ_c^2 as a function of γ_c^1, that is, $\gamma_c^2=f(\beta)=f(\gamma_c^1)$ (Fig. 3c). Similarly, the system exhibits bifurcating behaviour when γ is fixed ($\gamma=20$ in Fig. 3d,e). For the system with the given mutualistic strength $\gamma=20$, it has two critical values for competition: $\beta_c^1=2.11$ and $\beta_c^2=0.29$ for $x_0=0.1$ (Fig. 3d). This bifurcation phenomenon, that is, the

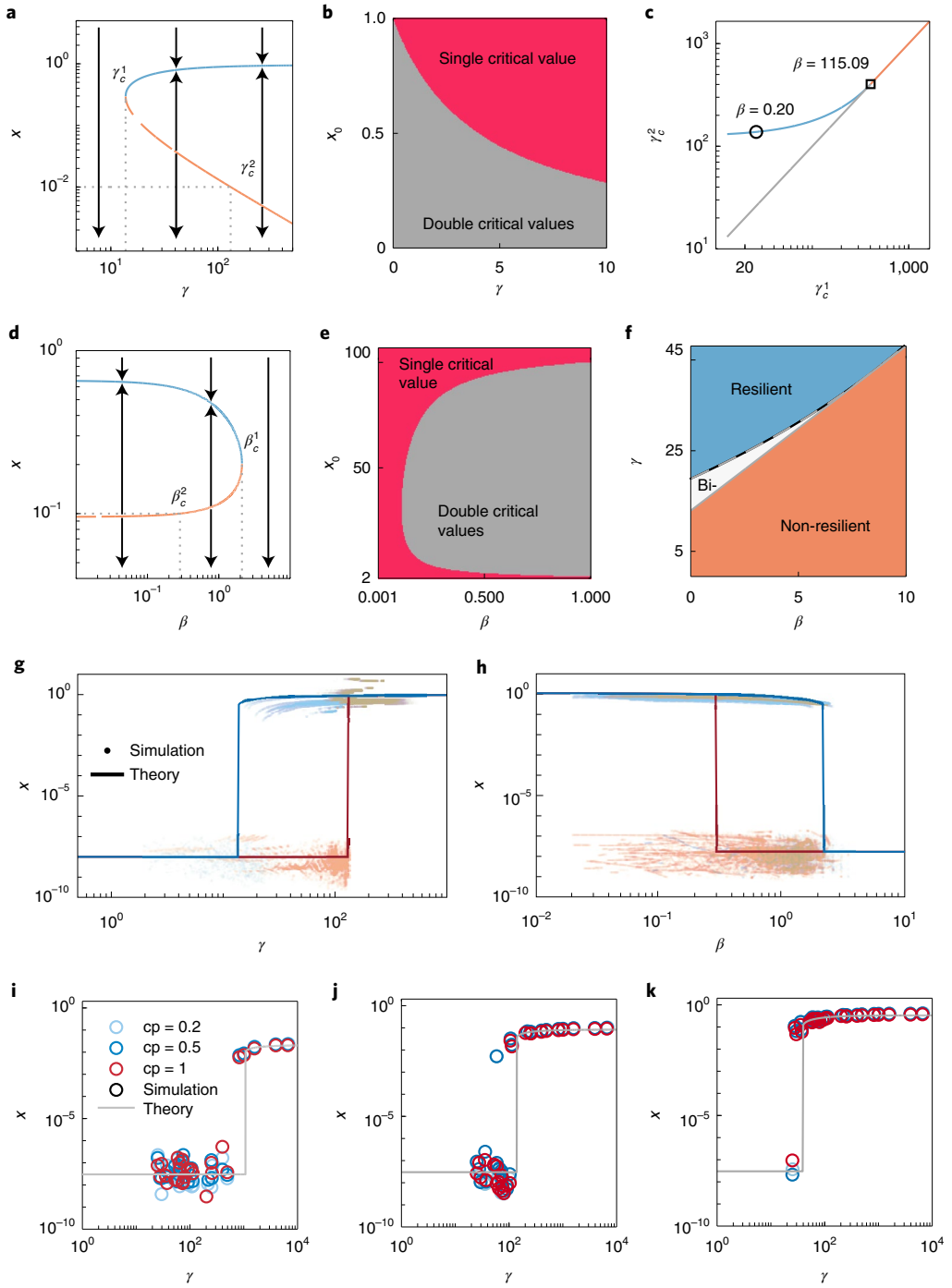

Fig. 3 | Detecting the resilience of mutualistic networks. We investigate the role of competition and mutualism on the formation of resilience patterns (equation (1) with $h = 0.2$, $\beta_s = 4$ and $\alpha = -1$). **a**, With $\beta = 0.2$, the one-dimensional system has two critical values for γ (the grey dotted lines): it could not stay high (blue line) if $\gamma < \gamma_c^1 = 13.74$ (the unidirectional arrows); it will leave the unstable fixed point (the orange dashed line) and lose its resilience finally if $\gamma < \gamma_c^2 = 131.67$ with $x_0 = 0.01$, otherwise become resilient (the bidirectional arrows). **b**, The existence of the second critical value γ_c^2 depends on x_0 and γ. **c**, γ_c^2 can be expressed as a function of γ_c^1 (blue line), which is stopped when $\gamma_c^2 < \gamma_c^1$ (orange line), depending on the value of β (open circle shows the critical values of γ with $\beta = 0.20$, while square shows those with $\beta = 115.09$). **d**, With $\gamma = 20$, $\beta_c^1 = 2.11$ and $\beta_c^2 = 0.29$ for $x_0 = 0.1$. **e**, With $\gamma = 20$, both x_0 and β influence the existence of critical values. **f**, With $x_0 = 0.1$, both β and γ influence the existence of critical values. **g**, For $\gamma \in [19.2, 20.8]$, 39 real systems (points for simulation results) facing perturbations are mapped to the universal resilience function (lines for theoretical prediction, 1D equation (4)), starting with different initial states (blue for $x_0 = 5$, red for $x_0 = 0.01$). **h**, For $\beta \in [0.18, 0.22]$, with different initial states (blue for $x_0 = 5$, red for $x_0 = 0.1$). **i**, For 28 real weighted networks with $h = 0.8$, we maintained the effective competition strength $\beta = 1.00$ but changed the competition topology by assigning three different linking probabilities (cp): 0.2 (light blue), 0.5 (blue) and 1 (red) and found that all results fit the predicted 1D resilience function (grey curve, equation (4)). **j**, $h = 0.5$, others as in **i**. **k**, $h = 0.2$, others as in **i**.

existence of β_c^2, depends on both the initial state x_0 and the mutualistic strength γ (Fig. 3e).

The finding shows that the mutualism factor γ, along with the competition factor β, maps the resilience space of mutualistic networks together. When setting $x_0 = 0.1$, the interactive effects between γ and β influence the resilience of the system together and separate the functional space of the mutualistic system (equation (4)) into three distinct regions (Fig. 3f). In the resilient state (blue region in Fig. 3f where $\gamma \geq \gamma_c^2(x_0 = 0.1) > \gamma_c^1$), there is only one stable state $x > 0$ to which the system recovers from perturbations. In the Bi-stable state (white region in Fig. 3f, $\gamma_c^1 \geq \gamma < \gamma_c^2(x_0 = 0.1)$), whether the system can recover from perturbations or not depends on its initial state. In the non-resilient state (orange region in Fig. 3f, $\gamma < \gamma_c^1 < \gamma_c^2(x_0 = 0.1)$), there is only one stable state $x = 0$ in which the system could not recover to $x > 0$ after perturbations.

Building on the theoretical mapping, we tested the ability of β and γ to detect the resilience of real ecological networks. For 28 weighted pollinator networks with mutualistic interactions (Supplementary Table 2), we randomly assign the competitive topology with the linking probability as 50% to explore the system's response to diverse perturbations. We fix β within a small range centred around 0.2, that is, $\beta \in [0.18, 0.22]$, aligning with the β value used to obtain the theoretical result in Fig. 3g. We then simulate the dynamical response of the system with two initial values: $x_0 = 5$ (blue dots in Fig. 3g, where the system falls to non-resilient state at the point that corresponds to γ_c^1) and $x_0 = 0.1$ (orange dots in Fig. 3g, where the system falls to non-resilient state at the point that corresponds to γ_c^2). Our resilience function can predict the behaviours of the systems (curves in Fig. 3g). We observe similar behaviours when fixing γ in a small range (Fig. 3h).

Next, we examine how different dynamics affect the biomass of a system at equilibrium. We set three different dynamical parameters with the saturating constant equal to $h = 0.8$, 0.5 and 0.2 in Fig. 3i–k, respectively. In each case, we set the competition typologies with the linking probability equal to 20% (light blue), 50% (blue) and 100% (red). The simulation results show that the 28 weighted systems converge onto the grey curve that is predicted by equation (4). More combinations of parameters, such as growth rate α, can be found in Extended Data Fig. 3 and Supplementary Fig. 16.

The results from the tests demonstrate that our one-dimensional function can go beyond mapping the resilience of mutualistic systems; it is able to converge complex behaviours into a one-dimensional system around the theoretical prediction. It thus provides a tool to predict seemingly unpredictable behaviours of the mutualistic systems that are impacted by a variety of perturbations and governed by different combinations of parameters. Moreover, this advancement is a critical foundation in calculating distances to possible tipping points in complex systems with mutualistic interactions, as well as developing an approach to comparing the distances across different systems in our next steps.

Reflecting the resilience of real-world ecosystems. Existing approaches and metrics are incapable of measuring the resilience of a high-dimensional system on the basis of spatiotemporal data due to the lack of an effective structural indicator. It prevents us from positioning a network from its possible tipping point or comparing the distances to tipping points from various systems on the same scale. Besides, the dearth of empirical data from ecological systems also adds difficulties in measuring distances to tipping points[33]; in most cases, we only have abundance and network data (Fig. 4a), reflecting mere snapshots of the states of mutualistic systems[52]. Here we attempt to use data on abundance and topology to predict real ecological systems' resilience.

We gathered literature and obtained species abundance data at eight locations worldwide (Fig. 4b; see Methods (Abundance data) and Extended Data Fig. 1). These species construct 54 mutualistic ecological networks, 51 of which have weighted topologies and 3 unweighted (see Supplementary Tables 3 and 4, respectively). Putting the real fraction of abundances of all plants $\mathbf{y}$, as the input of operator $\varkappa_2$, constructed by the real mutualistic topology M, we obtain the effective fraction of abundance $y_{\text{eff}} = \varkappa_2(\mathbf{y}) = \frac{1^\top M\mathbf{y}}{1^\top M1}$ for a mutualistic system (see Methods, Fraction and normalization).

We then calculate the geographical distribution of the effective fractions of abundances (y_{eff}) at the eight locations. The values of effective abundance y_{eff} come from locations Nahuel Huapi National Park in Argentina to Isenbjerg, denoted as A to H (see Extended Data Fig. 1). The two largest y_{eff} are in Argentina (location A) and Morne Seychellois National Park, Mahé (location B), which are both national parks. There are 47 mutualistic networks at location B, and thus, y_{eff} at this location is the average of the effective fraction of abundances of these systems (also see Supplementary Note 4 for more details). To understand whether the high-dimensional equation (1) is a potential dynamics rule for these networks, we used these abundance data and the 54 real ecological networks to estimate parameters for each network (see Methods, Parameter estimation). As shown in Fig. 4c, the excellent match between each species' abundance y_i and the simulated one y_i^s helps us to make the assumption that all these networks follow the same rules (equation (1)) and are thus potentially comparable.

As pointed out in ref. [53], there is a positive linear correlation between species abundance and nestedness. Thus, we test the performance of γ when predicting y_{eff} and compare the results to the ones measured by nestedness indicators. We compute the normalized NODF[54] (short for 'Nested Overlap and Decreasing Fill', a consistent metric for nestedness analysis in ecological systems; Fig. 4d), maximum Eigenvalue[55] (Fig. 4e) and γ (Fig. 4f) and then examine the correlation of these measures to the abundance of the plants. We find that γ shows higher correlation ($R^2 = 0.644^{***}$) compared with both nestedness measures ($R^2 = 0.297$ for normalized NODF and 0.538 for maximum eigenvalue) ($^{***}P < 0.001$). The residuals are shown in Fig. 4g. The results indicate that γ can be a more effective structural indicator to identify the crucial components from massive nodes and evaluate the current state of a system.

The scaling factor for recovery rates. After developing and demonstrating γ as an effective structural indicator for the state of mutualistic networks, our last step is to create a novel approach to compare the distances of different systems to their respective tipping points. The approach is a vital contribution because, to our best knowledge, no available methods can position two systems with entirely different parameters on the same scale for comparison purposes. In other words, existing approaches cannot position systems on the same scale and thus cannot evaluate which system is more endangered and, consequently, require prioritized resources. This limitation hinders the optimization of global resource allocation[56].

To demonstrate this critical limitation, we tested the performance of recovery rate[40] on indicating the resilience of a system. When a system approaches the possible tipping point (that is, the distance $\gamma - \gamma_c$ decreases), the recovery rate decreases and the autocorrelation variance increases as a result of the shrinkage in the attraction basin and a longer memory for perturbations[32,42]. Therefore, for a single one-dimensional system with fixed parameters, both measures can potentially capture the system's distance from its tipping point, as shown in Fig. 5a.

However, neither recovery rate nor autocorrelation can compare different systems with entirely different parameters. Our experiments demonstrate the limitation of the recovery rate approach: we choose three real ecological networks, parameterize dynamic roles through their real abundance data (see Methods, Parameter estimation for more details) and convert them into one-dimensional systems using equation (4). Although the three systems experience the

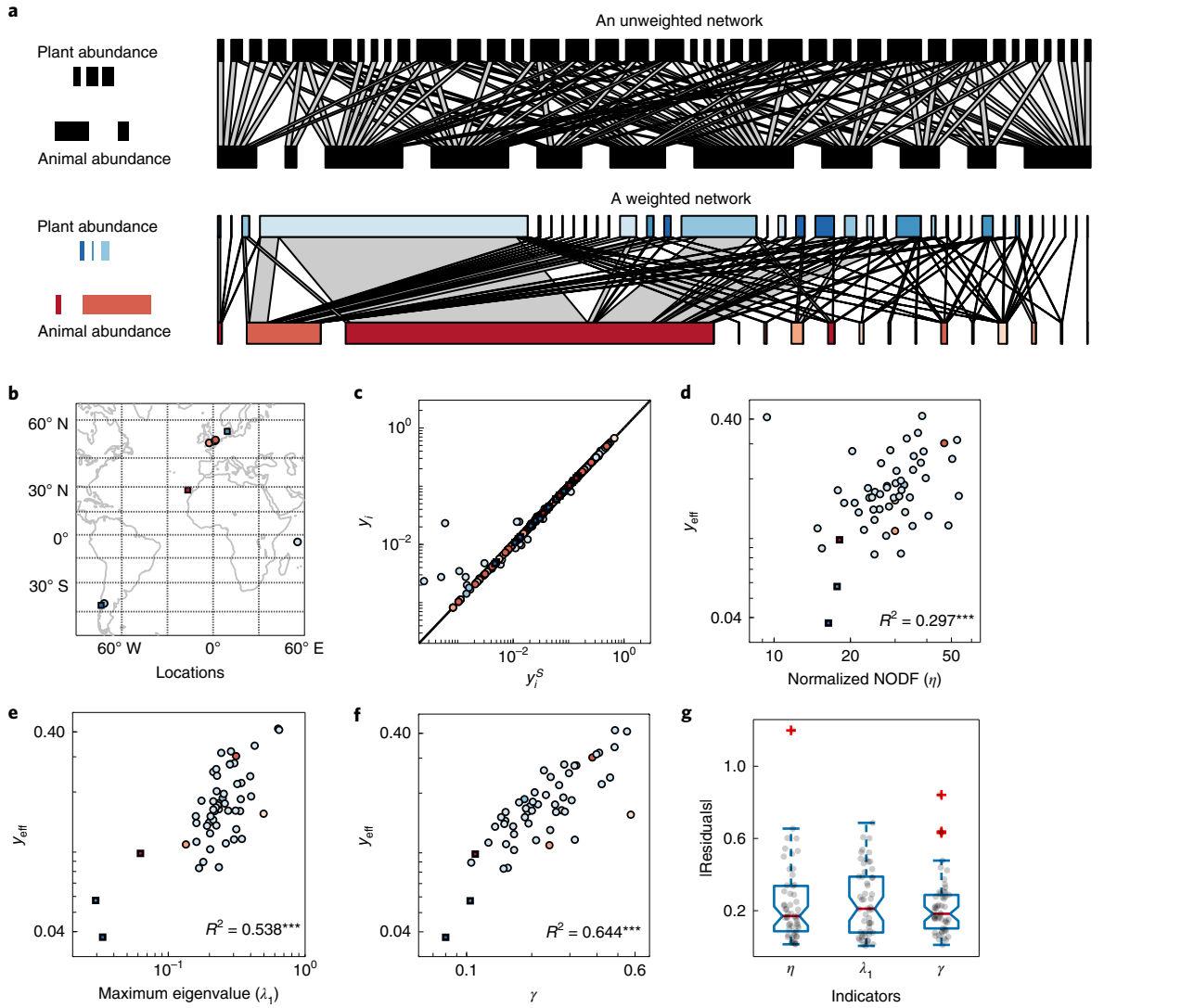

Fig. 4 | Detecting signals from real ecosystems. a, We show the adjacency matrix of a real weighted ecological network (Supplementary Table 3) and a real unweighted one (Supplementary Table 4), with the proportional abundance of each species indicated by the width of its corresponding block. **b**, Real pollinator networks (54) with the real proportional abundance of each plant, which come from 8 locations worldwide (8 colours, Extended Data Fig. 1), including 51 weighted networks (circle) and 3 unweighted ones (square). **c**, Assuming all the 54 real pollinator networks are governed by equation (1) with $h = 0.2$, we adjusted their dynamical parameters (α, β_s) to obtain the proportional abundances (y_i^s), which are extremely close to the real ones (y_i). **d**, Nestedness η vs the effective abundance y_{eff}. **e**, Maximum eigenvalue λ_1 vs the effective abundance y_{eff}. **f**, Effective mutualistic strength γ vs the effective abundance y_{eff}. **g**, We show the three indicators' ability to explain real abundance by comparing their residuals of linear correlation between indicators and effective abundances. In each box, there are 54 points (the effective abundance for 54 networks). The central red line indicates the median, the bottom and top edges of the box indicate the 25th and 75th percentiles, respectively, and the whiskers extend to the most extreme data points not considered as outliers (the outliers are marked with '+').

same levels of state perturbations (Fig. 5b), their distances to tipping points greatly differ (Fig. 5c).

To overcome this limitation, we employ our dimension-reduction approach and describe the tipping point γ_c as a function of dynamical parameters; thus, the distance to tipping point $\gamma - \gamma_c$ becomes a function of structure and dynamics, that is,

$$\gamma - \gamma_c = f(\alpha, \beta_w). \tag{5}$$

When the system is stable, the effective state of the whole system can be captured by

$$x_s = f(\alpha, \beta_w, \gamma). \tag{6}$$

The recovery rate is defined as the change rate from the stable state x_s after perturbation δ:

$$g(\delta x_s) = \frac{d\delta x_s}{dt} = f(\alpha, \beta_w, \gamma, \delta). \tag{7}$$

For equation (4), the recovery rate has the form

$$\begin{aligned} g(\delta x_s) &= \delta x_s \left(\alpha - \delta\beta_w x_s + \frac{\delta\gamma x_s}{1+\delta h\gamma x_s}\right) \\ &\approx \delta(1-\delta)\frac{1}{h^2}\left[\frac{(1+h\alpha)^2}{\beta_w} - \frac{\left(1+\sqrt{-h\alpha}\right)}{\gamma}\right]. \end{aligned} \tag{8}$$

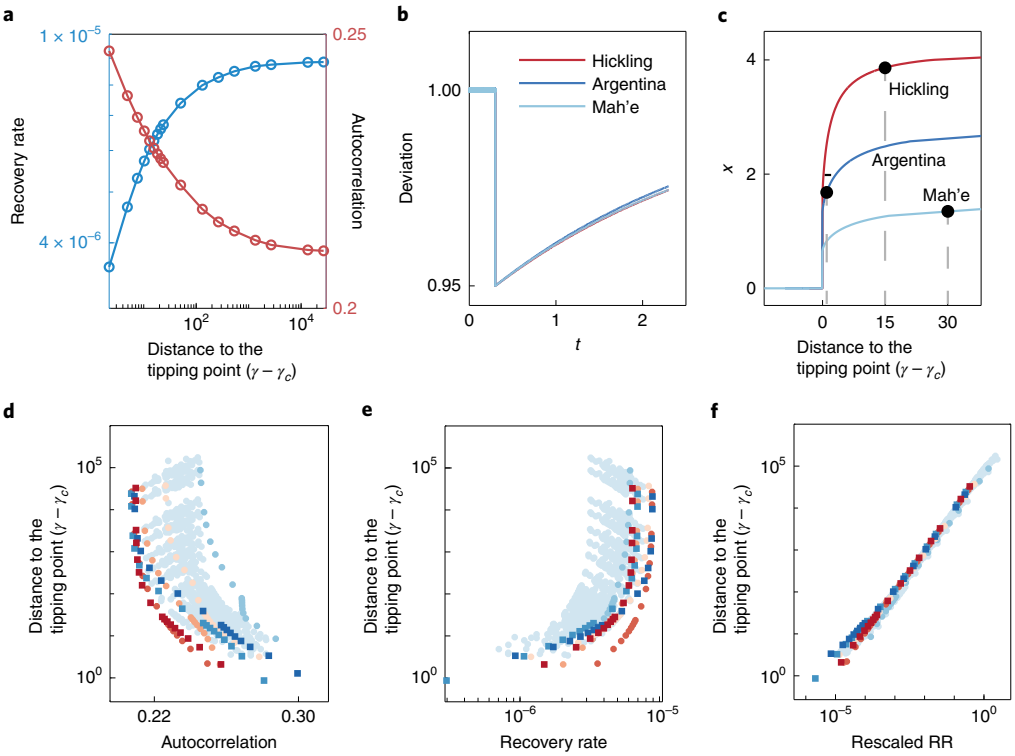

Fig. 5 | Early-warning signals predict distances to tipping points of ecosystems. a, A 1D system is forced, changing stochastically by adding white noise with 0.01 strength to equation (4) with $\alpha = -1$, $\beta_s = 1$, $h = 0.2$. When the system approaches its tipping point (the distance $\gamma - \gamma_c$ decreases), the basin of attraction shrinks. The system has a longer memory for perturbations (for example, the state is suddenly reduced by a factor of 0.95), resulting in a lower recovery rate (blue) and a higher autocorrelation (red). **b**, When the high-dimensional system collapses into a 1D one, we can observe how the system, after being disturbed, varies from its original stable state (derivation) as time (t) changes, allowing us to calculate the recovery rate for the system. **c**, Although the three systems (that is, mutualistic networks for the locations Argentina, Hickling and Mahé, respectively) are observed the same recovery rate after the same level of perturbation (**b**), their distances to tipping points are greatly differ (black dots). **d**, We obtain dynamical parameters for 54 real ecological networks and monitor how autocorrelation at lag 1 changes when an empirical system approaches its tipping point. **e**, We also monitor the recovery rate for each empirical system. **f**, The scaled recovery rate (RR) reflects the distance to the tipping point. Thus, we could evaluate how far different systems are to the loss of resilience.

with two approximations $g(\delta x_s) \approx \delta(1-\delta)\beta_w x_s^2$ and $x_s^2 \approx \frac{1}{h^2}[(\frac{1+h\alpha}{\beta_w})^2 - \frac{(1+\sqrt{-h\alpha})}{\beta_w \gamma}]$ (see more details in Supplementary Note 5).

Since both the distance $\gamma - \gamma_c$ (equation (5)) and the recovery rate (equation (7)) are functions of effective parameters α, β_w, γ, we can obtain the relationship between them as

$$\gamma - \gamma_c = \rho \times g(\delta x_s), \tag{9}$$

with the scaling factor

$$\rho = \frac{h^2 \beta_w \gamma}{\delta(1-\delta)(1+h\alpha)^2}. \tag{10}$$

The scaling factor ρ is a critical parameter since it contains multiple effective parameters, h, α, β_w and γ, extracted from a high-dimensional system. Therefore, ρ captures the dynamic behaviour of a disrupted high-dimensional system by mapping it to a one-dimensional one. Also, since ρ is uniquely determined by a given network, it not only predicts the distance to the tipping point of a single system but also compares the distances across multiple ones.

We demonstrate the applicability of our scaling factor ρ by applying it to the 54 real mutualistic networks used in Fig. 4. These systems have diverse resiliences since their dynamic parameters (α_i, β_{si} in equation (1)) and the interaction matrices (β_{ij}, γ_{ij}) are different. Note that the parameters of these networks were estimated using abundance data (see Methods, Parameter estimation for details). The coexistence of species can be captured using system parameters[44]; once the original parameters are determined, we can capture a system to its domain boundary, that is, the distance to tipping points. Then, we design simulations that run on both the original high-dimensional matrix and the converted one-dimensional system, which is useful to confirm that our method is applicable to high-dimensional systems. As shown in Fig. 5d, the seemingly chaotic behaviours are difficult to capture using autocorrelation. At the same $\gamma - \gamma_c$, systems can have entirely different autocorrelations, making it challenging to compare resilience across different systems. We monitor the changes in recovery rates in the same simulations and observe a similar pattern (Fig. 5e). In contrast, after applying our scaling factor ρ, the distances to tipping points are captured. The conversion transfers the dynamic behaviours into nearly linear ones, as shown in Fig. 5f, allowing us to uniquely determine a system's resilience and compare the converted recovery rates across different systems on the same scale.

Discussion

Ecosystems are becoming increasingly vulnerable with the intensification of climate change and thus, understanding their resilience and predicting their tipping points is a critical and challenging issue[57–59]. Suppose a uniform comparison of the resilience across different

systems around the world could be achieved. In that case, human beings could identify truly endangered communities in vulnerable areas and optimize global resource allocation[60]. This theory-based paper takes the first step towards achieving such global comparison, where our developed approach can position diverse systems on the same scale and consequently compare their resilience.

The study contributes to the understanding of the resilience of mutualistic systems in three aspects. First and foremost, we develop a novel scaling factor, ρ, that positions and compares multiple systems on a common scale. This approach unprecedentedly measures distances to tipping points of mutualistic networks with different parameters and topologies, comparing their resilience. Our study builds upon previous research in mutualistic network resilience, especially the works that examine critical tipping points in one network[31]. It is thus a vital contribution to the theories of critical transitions in mutualistic systems composed of more than one network. For real systems that could be approximated using equation (1), ρ may help optimize the allocation of resources according to their distances to the tipping point. If successfully validated by real-world data from ecological systems, our approach can also help protect vulnerable ecosystems and assist in designing global early-warning systems to cope with large-scale ecological crises.

Second, we quantify and explore the resilience of high-dimensional mutualistic networks by designing a single-dimensional structural indicator γ. Compared with established measures[55,61,62] used to capture the nestedness of ecosystems, the condensed values of γ show a high capability of mapping resilience of different systems with a one-dimensional function. The performance of γ makes it a potential structural indicator and thus contributes to the search for a universal indicator.

Lastly, we devise an approach to measure the distance of a system's current resilience to its tipping point. Our approach, assuming the dynamics of all systems follow equation (1), identifies the parameters of a system using abundance data, that is, a single snapshot of a system. The method makes it possible to obtain the tipping points (γ_c) of mutualistic networks without relying on time-series data[58].

Additionally, the study develops a method to estimate the parameters of ecological systems. Our method helps address the challenge in the real world: high-quality spatiotemporal data is too scarce to permit observation of the entire stochastic process of a system[63,64]. The abundance data provide only a snapshot of the state of a system. Our method estimates the parameters of real ecological networks on the basis of only their abundance data and the network topology, thus making it possible to monitor globally with limited real data.

Despite the broad discussions on empirical evidence of, as well as the ongoing efforts in searching for, critical thresholds in ecological systems, our model advances the capability of capturing and predicting such critical transitions. At a minimum, it provides a needed theoretical approach to understand systems whose behaviours fall into the applicability of our framework (see Methods, Applicability). In this paper, we study a theoretical model of an ecological system with competitive and mutualistic dynamics. We find that this model may have a tipping point, depending on the parameters. For example, if the intrinsic growth rate is larger than zero, there will be no tipping point. However, in this case our dimensional reduction method still works well (see Extended Data Fig. 3). For the case with a tipping point (that is, the intrinsic growth rate is smaller than zero), we can predict the distance to the tipping point using a rescaling factor.

Our study has limitations on heterogeneity and interspecific competition (see Extended Data Fig. 4). The prediction fails with large interspecific competition and high heterogeneity, necessitating future work allowing greater freedom. Additionally, holistic and empirical validation of our theory is still elusive and beyond the scope of this study. Observation data of thresholds in mutualistic networks will broaden the applicability of our theory in the future.

Beyond the application to ecosystems, our developed framework and operations can be extended to explore the resilience of other interdependent worldwide systems[65] (see Extended Data Fig. 5 and Supplementary Note 7 for supply-chain networks). Moreover, the work supports current efforts in the field and demonstrates the feasibility of devising a universal framework to quantify, predict and control mutualistic networks in an increasingly changing global environment.

Method

Complex systems described by interacting equations. We can approximate the behaviour of these complex systems by a set of interacting equations with high dimensionality:

$$\begin{aligned}\frac{dx_i^{\mathrm{I}}}{dt} &= F\left(x_i^{\mathrm{I}}\right) + \sum A_{ij} G\left(x_i^{\mathrm{I}}, x_j^{\mathrm{I}}\right) + \sum B_{ip} H\left(x_i^{\mathrm{I}}, x_p^{\mathrm{II}}\right)\\ \frac{dx_m^{\mathrm{II}}}{dt} &= P\left(x_m^{\mathrm{II}}\right) + \sum C_{mn} Q\left(x_m^{\mathrm{II}}, x_n^{\mathrm{II}}\right) + \sum D_{mk} R\left(x_m^{\mathrm{II}}, x_k^{\mathrm{I}}\right)\end{aligned}, \quad (11)$$

which describes the dynamic roles governing a system composed of Network I and Network II. The first term on the right-hand side of each equation (11) captures the self-dynamics of a component, the second term captures the competitive interactions between component i (m) and component j (n) within Network I (II), and the third term captures the mutualistic interactions between component i (m) and its interacting partners, p (k), from the other network. The nonlinear functions $F(\cdot)$, $G(\cdot)$, $H(\cdot)$, $P(\cdot)$, $Q(\cdot)$ and $R(\cdot)$ represent the dynamical laws governing components, while the connectivity matrices A, B, C and D describe the interactions between components. Their values are negative for competition and positive for mutualism.

Hypothesis. Assumption 1. Heterogeneity is not overly high. Since our method relies on the validity of the mean-field theory, overly high heterogeneity will make the method unable to predict the behaviour of the complex systems[67]. It is worth noting that the empirical network structures applied in Supplementary Tables 1–4 are of high heterogeneity. Also in Supplementary Note 3, it is shown that our method can tolerate large heterogeneity in parameter h.

Assumption 2. Interspecific competition is much smaller than self-competition, that is, $\beta_{ij} \ll \beta_{ii}$. Strong competition may lead to many stable fixed points in a system[68] because different combinations of species may become extinct depending on the initial conditions. Consequently, it brings high heterogeneity in the competition dynamics, which could make the mean-field theory inapplicable.

Dimensional reduction. In a network environment, each node's state is affected by its nearest neighbours through the interaction term. For a mutualistic network governed by equation (12), the interaction terms have the form $\sum_{j\neq i}^{N^{\mathrm{I}}} A_{ij} G\left(x_i^{\mathrm{I}}, x_j^{\mathrm{I}}\right)$.

$$\begin{aligned}\frac{dx_i^{\mathrm{I}}}{dt} &= F\left(x_i^{\mathrm{I}}\right) + \sum_{j\neq i}^{N^{\mathrm{I}}} A_{ij} G\left(x_i^{\mathrm{I}}, x_j^{\mathrm{I}}\right) + \sum_{p}^{N^{\mathrm{II}}} B_{ip} H\left(x_i^{\mathrm{I}}, x_p^{\mathrm{II}}\right),\\ \frac{dx_m^{\mathrm{II}}}{dt} &= P\left(x_m^{\mathrm{II}}\right) + \sum_{n\neq m}^{N^{\mathrm{II}}} C_{mn} Q\left(x_m^{\mathrm{II}}, x_n^{\mathrm{II}}\right) + \sum_{k}^{N^{\mathrm{I}}} D_{mk} R\left(x_m^{\mathrm{II}}, x_k^{\mathrm{I}}\right)\end{aligned} \quad (12)$$

For node i with s_i neighbours, $s_i \times \mathcal{L}(M, \mathbf{y})$ naturally incorporates the sum of nearest neighbours averaging procedure $\mathbf{y}$. Thus, equation (12) can be converted into equation (13) without much cost:

$$\begin{aligned}\frac{dx_i^{\mathrm{I}}}{dt} &= F\left(x_i^{\mathrm{I}}\right) + s_i^{\mathrm{I}} G\left(x_i^{\mathrm{I}}, \mathcal{L}\left(A, \mathbf{x}^{\mathrm{I}}\right)\right) + s_i^{\mathrm{I}} H\left(x_i^{\mathrm{Ic}}, \mathcal{L}\left(B, \mathbf{x}^{\mathrm{II}}\right)\right)\\ \frac{dx_m^{\mathrm{II}}}{dt} &= P\left(x_m^{\mathrm{II}}\right) + s_m^{\mathrm{II}} Q\left(x_m^{\mathrm{II}}, \mathcal{L}\left(C, \mathbf{x}^{\mathrm{II}}\right)\right) + s_m^{\mathrm{IIc}} R\left(x_m^{\mathrm{II}}, \mathcal{L}\left(D, \mathbf{x}^{\mathrm{I}}\right)\right)\end{aligned} \quad (13)$$

Here we name $x_{\mathrm{eff}}^{J}=\mathcal{L}\left(A,\mathbf{x}^{\mathrm{I}}\right)$, $x_{\mathrm{eco}}^{\mathrm{I}}=\mathcal{L}\left(B,\mathbf{x}^{\mathrm{II}}\right)$, $x_{\mathrm{eff}}^{\mathrm{II}}=\mathcal{L}\left(C,\mathbf{x}^{\mathrm{II}}\right)$ and $x_{\mathrm{eco}}^{\mathrm{I}}=\mathcal{L}\left(D,\mathbf{x}^{\mathrm{I}}\right)$, indicating the mean-field weighted states of x. Then the four scalars can be obtained by solving the following equations:

$$\begin{aligned}
\frac{dx_{\mathrm{eff}}^{\mathrm{I}}}{dt}&=F\left(x_{\mathrm{eff}}^{\mathrm{I}}\right)+\mathcal{L}\left(A,\mathbf{s}^{\mathrm{I}}\right)G\left(x_{\mathrm{eff}}^{\mathrm{I}},x_{\mathrm{eff}}^{\mathrm{I}}\right)+\mathcal{L}\left(B,\mathbf{s}^{\mathrm{I}}\right)H\left(x_{\mathrm{eff}}^{\mathrm{I}},x_{\mathrm{eco}}^{\mathrm{II}}\right)\\
\frac{dx_{\mathrm{eff}}^{\mathrm{II}}}{dt}&=P\left(x_{\mathrm{eff}}^{\mathrm{II}}\right)+\mathcal{L}\left(C,\mathbf{s}^{\mathrm{II}}\right)Q\left(x_{\mathrm{eff}}^{\mathrm{II}},x_{\mathrm{eff}}^{\mathrm{II}}\right)+\mathcal{L}\left(D,\mathbf{s}^{\mathrm{IIc}}\right)R\left(x_{\mathrm{eff}}^{\mathrm{II}},x_{\mathrm{eco}}^{\mathrm{I}}\right)\\
\frac{dx_{\mathrm{eco}}^{\mathrm{I}}}{dt}&=F\left(x_{\mathrm{eco}}^{\mathrm{I}}\right)+\mathcal{L}\left(A,\mathbf{s}^{\mathrm{I}}\right)G\left(x_{\mathrm{eco}}^{\mathrm{I}},x_{\mathrm{eff}}^{\mathrm{I}}\right)+\mathcal{L}\left(B,\mathbf{s}^{\mathrm{I}}\right)H\left(x_{\mathrm{eco}}^{\mathrm{I}},x_{\mathrm{eco}}^{\mathrm{II}}\right)\\
\frac{dx_{\mathrm{eco}}^{\mathrm{II}}}{dt}&=P\left(x_{\mathrm{eco}}^{\mathrm{II}}\right)+\mathcal{L}\left(C,\mathbf{s}^{\mathrm{II}}\right)Q\left(x_{\mathrm{eco}}^{\mathrm{II}},x_{\mathrm{eff}}^{\mathrm{II}}\right)+\mathcal{L}\left(D,\mathbf{s}^{\mathrm{IIc}}\right)R\left(x_{\mathrm{eco}}^{\mathrm{II}},x_{\mathrm{eco}}^{\mathrm{I}}\right)
\end{aligned}\tag{14}$$

Knowing the effective states through equation (14), equation (13) is decoupled and the state for every node can also be solved.

For mutualistic networks, a system consisting of more than one network ($\beta^{(P)}$, $\beta^{(A)}$, $\gamma^{(P)}$, $\beta^{(A)}$ in equation (1)), the state of a node is affected by the neighbours in the same network as well as the neighbours in different networks. Therefore, we characterize four effective states of the system using the average nearest-neighbour activity

$$\begin{aligned}
P^{\mathrm{P}}&=\mathcal{L}(\beta^{(P)},P),A^{\mathrm{A}}=\mathcal{L}(\beta^{(A)},A),P^{\mathrm{A}}\\
&=\mathcal{L}(\gamma^{(A)},P),A^{\mathrm{P}}=\mathcal{L}(\gamma^{(P)},A),
\end{aligned}\tag{15}$$

where P^{P} (A^{A}) reflects the average state of plants (animals) from the viewpoint of plants (animals) themselves, while P^{A} (A^{P}) reflects the average state from the viewpoint of animals (plants). Similarly, we characterize the effective states for the dynamical parameters (α, β_s) and the structural properties $\mathbf{s}$, which indicate the number of nearest neighbours in one structure, that is, $\mathbf{s}^{\mathrm{I}}=(s_i^{\mathrm{I}})=(\sum_j\beta_{ij}^{(P)})$, $\mathbf{s}^{\mathrm{II}}=(s_i^{\mathrm{II}})=(\sum_j\beta_{ij}^{(A)})$, $\mathbf{s}^{\mathrm{Ic}}=(s_i^{\mathrm{Ic}})=(\sum_k\gamma_{ik}^{(P)})$, $\mathbf{s}^{\mathrm{IIc}}=(s_i^{\mathrm{Ic}})=(\sum_k\gamma_{ik}^{(A)})$, as shown in Table 1.

In sum, the input matrix M of the operator $\mathcal{L}(M,\mathbf{y})$ can be the inner-structure in a network and the inter-structure across networks, while the input vector $\mathbf{y}$ can be the states, the parameter in the dynamic functions, as well as the structural information for each species. This allows us to abstract a high-dimensional system (equation (1)) by a four-dimensional resilience function (equation (3)).

Further, from the abstracted information above, we assemble a new matrix Z as

$$Z=\begin{bmatrix}\beta^{\mathrm{PP}} & 0 & 0 & \gamma^{\mathrm{PP}}\\ 0 & \beta^{\mathrm{PP}} & \gamma^{\mathrm{AA}} & 0\\ \beta^{\mathrm{PA}} & 0 & 0 & \gamma^{\mathrm{PA}}\\ 0 & \beta^{\mathrm{AP}} & \gamma^{\mathrm{AP}} & 0\end{bmatrix}.\tag{16}$$

Putting matrix Z as the input matrix of operator $\mathcal{L}(M,\mathbf{y})$, there will be a one-dimensional equation

$$\frac{dx}{dt}=x\left[\alpha+(\beta_s+\beta)x+\frac{\gamma x}{1+h\gamma x}\right],\tag{17}$$

where x captures the effective abundance for both plants and animals (more details can be seen in Table 2).

For the system consisting of more than one network (that is, $\beta^{(P)}$, $\beta^{(A)}$, $\gamma^{(P)}$, $\beta^{(A)}$ in equation (1)), the state of a node is affected by the neighbours in the same network as well as the ones in different networks. However, the existing approach[31] only works with one network. Therefore, we expand our previous work[31] and develop a two-step compression approach. The first step compresses the original interaction matrix (such as $y=\mathcal{L}(\beta^{(P)},\mathbf{y})$) as the case with just one network. The second step reconstructs a matrix Z with the scalar y obtained from the first step. For a system consisting of n networks, the matrix Z is $n\times n$ dimensional.

Data of networks. To construct mutualistic networks, we collected data on symbiotic ecological interactions from the 'Web of life' website[66], including

(i) Supplementary Table 1, 39 unweighted pollination networks. We used these networks in Fig. 2 in the manuscript and Supplementary Figs. 8–15.
(ii) Supplementary Table 2, 28 weighted pollination networks. We used these networks in Fig. 3 in the manuscript and Supplementary Fig. 16.
(iii) Supplementary Table 3, 51 weighted ecological networks with abundance data. We applied these network data to Figs. 4 and 5 in the manuscript and Supplementary Figs. 19–23 and Table 6.
(iv) Supplementary Table 4, 3 unweighted ecological networks with abundance data. We applied these network data to Figs. 4 and 5 in the manuscript and Supplementary Figs. 19–23 and Table 6.

Abundance data. We looked through papers that listed pollination networks in the 'Web of life'[66]. Seven papers were found[69–75], each of which recorded real data on abundance. We obtained a total of 54 networks with data on abundance for plant species, including 51 with a weighted topology (Supplementary Table 3) and 3 with an unweighted topology (Supplementary Table 4). These networks were spread in eight locations worldwide (Supplementary Table 5).

Proportion and normalization. Since some papers only contain proportional abundance, that is, the ratio of one species' abundance to the total abundance of all species, instead of the value of abundance, we used the proportional abundance y of each plant in this study. To consider all networks with data on abundance (Supplementary Tables 3 and 4) consistently, we divided one network by the sum of all elements to obtain the relationship between network structure and species abundance, as shown in Fig. 4.

Applicability. Our model has wide applicability. Although we computed the effective parameters using the original state variables in this study, the information is not a prerequisite to use our model. In fact, our assumption is that all systems are resilient at the time the abundance data were obtained. Thus, the model can be applied as long as the original abundance values are at high levels. However, it is worth noting that although our theoretical model does not inherently assume $\beta_{ij}\ll\beta_{ii}$ ($i\neq j$), it is necessary for our model to operate under such condition (see Extended Data Fig. 4a,b for the allowed range of β_{ij}). This is because our result is based on the validity of the mean-field theory, which could not be applied to a system with high heterogeneity (see ref. [31] for more discussion on this limitation).

Parameter estimation. Assuming all pollinator networks follow dynamics as in equation (1) without competition, we can simulate species abundance with interaction topology (γ_{ij}) and parameters of each species (α_i and β_{si}). In turn, one can estimate parameters with a given value of abundance and interaction topology. The specific process of parameter estimation is: first, we set the initial values of α_i for all species as -1 and β_{si} as 1; second, we computed the abundances for certain parameters and calculated the proportional abundances; third, we compared these proportional abundances of plants to the real ones and counted the sum Err. If $\mathrm{Err}>1\times10^{-6}$, we adjusted the values of these parameters, went back to the second step, and tested again. The process ended when an additional adjustment on the parameters could not decrease Err anymore. The estimated parameters for each species in all 54 networks are publicly

available (see Data availability). Assuming all the 54 real pollinator networks are governed by equation (1) with $h=0.2$, we adjusted their dynamical parameters (α, β_s) to obtain the proportional abundances (y_i^s), which are extremely close to the real ones (y_i), as shown in Fig. 4c.

Statistics. For each boxplot in this paper, the central mark indicates the median, the bottom and top edges of the box indicate the 25th and 75th percentiles, respectively, and the whiskers extend to the most extreme data points not considered outliers (the outliers are marked with '+').

Reporting summary. Further information on research design is available in the Nature Research Reporting Summary linked to this article.

Data availability

All network and abundance data can be accessed through https://doi.org/10.5281/zenodo.6784072.

Code availability

All code used in this study is available on Zenodo at https://doi.org/10.5281/zenodo.6784072.

Received: 7 April 2021; Accepted: 14 July 2022;
Published online: 29 August 2022

References

1. Aizen, M. A., Sabatino, M. & Tylianakis, J. M. Specialization and rarity predict nonrandom loss of interactions from mutualist networks. *Science* **335**, 1486–1489 (2012).
2. Aanen, D. K. et al. The evolution of fungus-growing termites and their mutualistic fungal symbionts. *Proc. Natl Acad. Sci. USA* **99**, 14887–14892 (2002).
3. Lello, J., Boag, B., Fenton, A., Stevenson, I. R. & Hudson, P. J. Competition and mutualism among the gut helminths of a mammalian host. *Nature* **428**, 840–844 (2004).
4. Jaeggi, A. V. & Gurven, M. Natural cooperators: food sharing in humans and other primates. *Evol. Anthropol.* **22**, 186–195 (2013).
5. Van Der Maas, H. L., Kan, K.-J., Marsman, M. & Stevenson, C. E. Network models for cognitive development and intelligence. *J. Intell.* **5**, 16 (2017).
6. Bascompte, J. & Jordano, P. Plant-animal mutualistic networks: the architecture of biodiversity. *Annu. Rev. Ecol. Evol. Syst.* **38**, 567–593 (2007).
7. Bastolla, U. et al. The architecture of mutualistic networks minimizes competition and increases biodiversity. *Nature* **458**, 1018 (2009).
8. Valverde, S. et al. The architecture of mutualistic networks as an evolutionary spandrel. *Nat. Ecol. Evol.* **2**, 94–99 (2018).
9. Vizentin-Bugoni, J. et al. Structure, spatial dynamics, and stability of novel seed dispersal mutualistic networks in Hawai'i. *Science* **364**, 78–82 (2019).
10. Bascompte, J. Disentangling the web of life. *Science* **325**, 416–419 (2009).
11. Liu, X. et al. Network resilience. *Phys. Rep.* **971**, 1–108 (2022).
12. Rezende, E. L., Lavabre, J. E., Guimarães, P. R., Jordano, P. & Bascompte, J. Non-random coextinctions in phylogenetically structured mutualistic networks. *Nature* **448**, 925–928 (2007).
13. Pocock, M. J., Evans, D. M. & Memmott, J. The robustness and restoration of a network of ecological networks. *Science* **335**, 973–977 (2012).
14. Fowler, J. H. & Christakis, N. A. Cooperative behavior cascades in human social networks. *Proc. Natl Acad. Sci. USA* **107**, 5334–5338 (2010).
15. May, R. M., Levin, S. A. & Sugihara, G. Complex systems: ecology for bankers. *Nature* **451**, 893–894 (2008).
16. Thébault, E. & Fontaine, C. Stability of ecological communities and the architecture of mutualistic and trophic networks. *Science* **329**, 853–856 (2010).
17. Berdugo, M. et al. Global ecosystem thresholds driven by aridity. *Science* **367**, 787–790 (2020).
18. Diaz, R. J. & Rosenberg, R. Spreading dead zones and consequences for marine ecosystems. *Science* **321**, 926–929 (2008).
19. Biggs, R. O., Peterson, G. & Rocha, J. C. The regime shifts database: a framework for analyzing regime shifts in social-ecological systems. *Ecol. Soc.* **23**, 3 (2018).
20. Walker, B. & Meyers, J. A. Thresholds in ecological and social-ecological systems: a developing database. *Ecol. Soc.* **9**, 2 (2004).
21. Hirota, M., Holmgren, M., Van Nes, E. H. & Scheffer, M. Global resilience of tropical forest and savanna to critical transitions. *Science* **334**, 232–235 (2011).
22. Barnosky, A. D. et al. Approaching a state shift in earth's biosphere. *Nature* **486**, 52–58 (2012).
23. Dakos, V. & Bascompte, J. Critical slowing down as early warning for the onset of collapse in mutualistic communities. *Proc. Natl Acad. Sci. USA* **111**, 17546–17551 (2014).
24. Lever, J. J., van Nes, E. H., Scheffer, M. & Bascompte, J. The sudden collapse of pollinator communities. *Ecol. Lett.* **17**, 350–359 (2014).
25. Lever, J. J. et al. Foreseeing the future of mutualistic communities beyond collapse. *Ecol. Lett.* **23**, 2–15 (2020).
26. Hillebrand, H. et al. Thresholds for ecological responses to global change do not emerge from empirical data. *Nat. Ecol. Evol.* **4**, 1502–1509 (2020).
27. Dudney, J. & Suding, K. N. The elusive search for tipping points. *Nat. Ecol. Evol.* **4**, 1449–1450 (2020).
28. Scheffer, M. et al. Anticipating critical transitions. *Science* **338**, 344–348 (2012).
29. Martin, S., Deffuant, G. & Calabrese, J. M. in *Viability and Resilience of Complex Systems* (eds. Deffuant, G., & Gilbert, N.) 15–36 (Springer, 2011).
30. Cohen, R., Erez, K., Ben-Avraham, D. & Havlin, S. Resilience of the internet to random breakdowns. *Phys. Rev. Lett.* **85**, 4626–4628 (2000).
31. Gao, J., Barzel, B. & Barabási, A.-L. Universal resilience patterns in complex networks. *Nature* **530**, 307–312 (2016).
32. Scheffer, M. et al. Early-warning signals for critical transitions. *Nature* **461**, 53–59 (2009).
33. Boettiger, C. & Hastings, A. Quantifying limits to detection of early warning for critical transitions. *J. R. Soc. Interface* **9**, 2527–2539 (2012).
34. Blanchard, J. L. A rewired food web. *Nature* **527**, 173–174 (2015).
35. Campbell, C., Yang, S., Shea, K. & Albert, R. Topology of plant-pollinator networks that are vulnerable to collapse from species extinction. *Phys. Rev. E* **86**, 021924 (2012).
36. Revilla, T. A., Encinas-Viso, F. & Loreau, M. Robustness of mutualistic networks under phenological change and habitat destruction. *Oikos* **124**, 22–32 (2015).
37. Vizentin-Bugoni, J. et al. Ecological correlates of species' roles in highly invaded seed dispersal networks. *Proc. Natl Acad. Sci. USA* **118**, (2021).
38. Whanpetch, N. et al. Temporal changes in benthic communities of seagrass beds impacted by a tsunami in the Andaman Sea, Thailand. *Estuar. Coast. Shelf Sci.* **87**, 246–252 (2010).
39. Orth, R. J. et al. Restoration of seagrass habitat leads to rapid recovery of coastal ecosystem services. *Sci. Adv.* **6**, eabc6434 (2020).
40. Veraart, A. J. et al. Recovery rates reflect distance to a tipping point in a living system. *Nature* **481**, 357–359 (2012).
41. Dai, L., Vorselen, D., Korolev, K. S. & Gore, J. Generic indicators for loss of resilience before a tipping point leading to population collapse. *Science* **336**, 1175–1177 (2012).
42. Dakos, V., van Nes, E. H., d'Odorico, P. & Scheffer, M. Robustness of variance and autocorrelation as indicators of critical slowing down. *Ecology* **93**, 264–271 (2012).
43. van Belzen, J. et al. Vegetation recovery in tidal marshes reveals critical slowing down under increased inundation. *Nat. Commun.* **8**, 15811 (2017).
44. Rohr, R. P., Saavedra, S. & Bascompte, J. On the structural stability of mutualistic systems. *Science* **345**, 1253497 (2014).
45. Wright, D. H. A simple, stable model of mutualism incorporating handling time. *Am. Nat.***134**, 664–667 (1989).
46. Newman, M. E. J. *Networks: An Introduction* (Oxford Univ. Press, 2010).
47. Jiang, J. et al. Predicting tipping points in mutualistic networks through dimension reduction. *Proc. Natl Acad. Sci. USA* **115**, E639–E647 (2018).
48. Gao, J., Buldyrev, S. V., Stanley, H. E. & Havlin, S. Networks formed from interdependent networks. *Nat. Phys.* **8**, 40–48 (2012).
49. May, R. M. Thresholds and breakpoints in ecosystems with a multiplicity of stable states. *Nature* **269**, 471–477 (1977).
50. Moreno, Y., Pastor-Satorras, R., Vázquez, A. & Vespignani, A. Critical load and congestion instabilities in scale-free networks. *Europhys. Lett.* **62**, 292–298 (2003).
51. Martinez, N. D., Williams, R. J., Dunne, J. A. & Pascual, M. in *Ecological Networks: Linking Structure to Dynamics in Food Webs* (eds. Pascual, M., Dunne, J. A., & Dunne, J. A.) 163–185 (Oxford University Press, 2006).
52. Chen, S., O'Dea, E. B., Drake, J. M. & Epureanu, B. I. Eigenvalues of the covariance matrix as early warning signals for critical transitions in ecological systems. *Sci. Rep.* **9**, 1–14 (2019).
53. Suweis, S., Simini, F., Banavar, J. R. & Maritan, A. Emergence of structural and dynamical properties of ecological mutualistic networks. *Nature* **500**, 449–452 (2013).
54. Mariani, M. S., Ren, Z.-M., Bascompte, J. & Tessone, C. J. Nestedness in complex networks: observation, emergence, and implications. *Phys. Rep.* **813**, 1–90 (2019).

55. Staniczenko, P. P., Kopp, J. C. & Allesina, S. The ghost of nestedness in ecological networks. *Nat. Commun.* **4**, 1–6 (2013).
56. Marsh, H. et al. Optimizing allocation of management resources for wildlife. *Conserv. Biol.* **21**, 387–399 (2007).
57. Dakos, V. et al. Slowing down as an early warning signal for abrupt climate change. *Proc. Natl Acad. Sci. USA* **105**, 14308–14312 (2008).
58. Reyer, C. P. et al. Forest resilience and tipping points at different spatio-temporal scales: approaches and challenges. *J. Ecol.* **103**, 5–15 (2015).
59. Dakos, V. et al. Ecosystem tipping points in an evolving world. *Nat. Ecol. Evol.* **3**, 355–362 (2019).
60. Hurwicz, L. The design of mechanisms for resource allocation. *Am. Econ. Rev.* **63**, 1–30 (1973).
61. Almeida-Neto, M. & Ulrich, W. A straightforward computational approach for measuring nestedness using quantitative matrices. *Environ. Model. Softw.* **26**, 173–178 (2011).
62. Atmar, W. & Patterson, B. D. The measure of order and disorder in the distribution of species in fragmented habitat. *Oecologia* **96**, 373–382 (1993).
63. Kéfi, S. et al. Spatial vegetation patterns and imminent desertification in Mediterranean arid ecosystems. *Nature* **449**, 213–217 (2007).
64. Dakos, V., van Nes, E. H., Donangelo, R., Fort, H. & Scheffer, M. Spatial correlation as leading indicator of catastrophic shifts. *Theor. Ecol.* **3**, 163–174 (2010).
65. Buldyrev, S. V., Parshani, R., Paul, G., Stanley, H. E. & Havlin, S. Catastrophic cascade of failures in interdependent networks. *Nature* **464**, 1025–1028 (2010).
66. *Web of Life, Ecological Networks Database* (Bascompte Lab, accessed 12 June 2017); http://www.web-of-life.es/map.php?type=5/
67. Gleeson, J. P., Melnik, S., Ward, J. A., Porter, M. A. & Mucha, P. J. Accuracy of mean-field theory for dynamics on real-world networks. *Phys. Rev. E* **85**, 026106 (2012).
68. Strogatz, S. H. *Nonlinear Dynamics and Chaos: with Applications to Physics, Biology, Chemistry, and Engineering* (CRC Press, 2018).
69. Vázquez, D. P. *Interactions Among Introduced Ungulates, Plants, and Pollinators: a Field Study in the Temperate Forest of the Southern Andes* PhD thesis, University of Tennessee (2002).
70. Kaiser-Bunbury, C. N., Vázquez, D. P., Stang, M. & Ghazoul, J. Determinants of the microstructure of plant-pollinator networks. *Ecology* **95**, 3314–3324 (2014).
71. Memmott, J. The structure of a plant-pollinator food web. *Ecol. Lett.* **2**, 276–280 (1999).
72. Dicks, L., Corbet, S. & Pywell, R. Compartmentalization in plant-insect flower visitor webs. *J. Anim. Ecol.* **71**, 32–43 (2002).
73. SMITH-RAMÍREZ, C., Martinez, P., Nunez, M., González, C. & Armesto, J. J. Diversity, flower visitation frequency and generalism of pollinators in temperate rain forests of Chiloé Island, Chile. *Bot. J. Linn. Soc.* **147**, 399–416 (2005).
74. Dupont, Y. L., Hansen, D. M. & Olesen, J. M. Structure of a plant-flower-visitor network in the high-altitude sub-alpine desert of Tenerife, Canary Islands. *Ecography* **26**, 301–310 (2003).
75. Dupont, Y. L. & Olesen, J. M. Ecological modules and roles of species in heathland plant-insect flower visitor networks. *J. Anim. Ecol.* **78**, 346–353 (2009).

Acknowledgements

W.Z. acknowledges support from the National Natural Science Foundation of China (grant nos. 61702200, 61473183, U1509211 and 61627810) and National Key R&D Program of China grant no. 2017YFE0128500. J.G. acknowledges the support of the USA National Science Foundation under Grant No. 2047488, and the Rensselaer-IBM AI Research Collaboration.. Q.W. was partially supported by the US National Science Foundation (grant no. 1761950 and 2125326). We sincerely thank J. Bascompte for early discussion and detailed suggestions that helped improve our paper.

Author contributions

All authors designed and conducted the research. H.Z. and J.G. performed the analytical and numerical calculations. H.Z., Q.W. and J.G. carried out analysis and interpreted the data. J.G. led the writing of the manuscript.

Competing interests

The authors declare no competing interests.

Additional information

Extended data is available for this paper at https://doi.org/10.1038/s41559-022-01850-8.

Supplementary information The online version contains supplementary material available at https://doi.org/10.1038/s41559-022-01850-8.

Correspondence and requests for materials should be addressed to Jianxi Gao.

Peer review information *Nature Ecology and Evolution* thanks György Barabás, Axel Rossberg and the other, anonymous, reviewer(s) for their contribution to the peer review of this work.

Reprints and permissions information is available at www.nature.com/reprints.

Publisher's note Springer Nature remains neutral with regard to jurisdictional claims in published maps and institutional affiliations.

LOC	No.	ID	Ref.	Address	LAT	LON
A	7	M_PL_051	[69]	Nahuel Huapi National Park, Argentina	-41.08	-71.53
B	8-54	M_PL_061	[70]	Morne Seychellois National Park, Mahé	-4.678	55.43
C	3	M_PL_0017	[71]	Bristol, England	51.57	-2.59
D	1	M_PL_006	[72]	Hickling, Norfolk, UK	52.76	1.58
E	5	M_PL_034	[73]	Chiloe, Chile	-42.00	-73.58
F	2	M_PL_007	[72]	Shelfanger, Norfolk, UK	52.41	1.10
G	4	M_PL_008	[74]	Tenerife, Canary Islands	28.22	-16.63
H	6	M_PL_047	[75]	Isenbjerg	56.07	9.27

Extended Data Fig. 1 | 54 real ecological networks with abundance values from 8 locations. We obtained 54 pollination networks with real proportional abundances from references listed above ('Ref.'), including 51 weighted networks (Table S3) and 3 unweighted ones (Table S4), spread in 8 locations world-wide. We sorted the effective abundance ratio decently as A - H. 'ID' is the network's code shown in 'web of life'[66], 'LAT' refers to the latitude of one location, and 'LONG' refers to its longitude.

No.	ID	$\|P\| * \|A\|$	$\|links\|$	C	H_P	H_A	γ	$\langle$err$\rangle$
1	M_PL_001	80*97	356	0.091753	8.660303	5.4783	59.38936	0.033534
2	M_PL_002	41*62	193	0.151849	3.739208	3.540806	44.53535	0.02904
3	M_PL_003	36*25	81	0.18	1.8483	0.954045	34.61865	0.033047
4	M_PL_005	91*270	918	0.074725	12.09665	22.37424	85.83789	0.075643
5	M_PL_006	11*5	24	0.872727	1.812821	0.702073	31.7511	0.038756
6	M_PL_007	28*82	250	0.21777	4.699554	5.589613	52.29448	0.034352
7	M_PL_008	11*38	106	0.507177	1.851186	2.262785	40.64927	0.028426
8	M_PL_009	24*118	242	0.170904	3.364109	4.853003	43.50656	0.045027
9	M_PL_010	31*76	456	0.387097	8.751467	6.343079	78.59856	0.037105
10	M_PL_011	14*13	52	0.571429	3.256185	0.886577	39.56818	0.033216
11	M_PL_012	29*55	145	0.181818	3.707286	7.191192	53.2207	0.032957
12	M_PL_013	16*44	278	0.789773	5.351415	4.688446	75.56421	0.035748
13	M_PL_014	28*80	178	0.158929	1.422533	10.69497	45.53219	0.034249
14	M_PL_015	130*663	2930	0.067989	18.24504	20.46229	105.1997	0.134177
15	M_PL_016	26*179	412	0.177052	4.315672	8.838581	56.45261	0.066942
16	M_PL_017	19*186	425	0.240521	3.866467	14.69992	56.1374	0.067596
17	M_PL_018	39*105	383	0.187057	7.31953	6.074937	61.45058	0.045413
18	M_PL_019	30*236	671	0.189548	5.510681	24.26356	66.86169	0.085705
19	M_PL_020	19*90	189	0.221053	1.806237	12.07049	46.96589	0.033203
20	M_PL_021	90*676	1192	0.039185	4.409285	16.98968	63.31119	0.109679
21	M_PL_022	21*45	83	0.175661	1.005965	1.946115	33.48591	0.034728
22	M_PL_023	20*70	122	0.174286	1.442396	5.791987	38.34417	0.038591
23	M_PL_024	37*225	590	0.141742	7.939882	9.724699	68.66649	0.076686
24	M_PL_025	14*35	86	0.35102	2.125964	2.738147	39.70423	0.028032
25	M_PL_026	99*51	198	0.078431	5.299093	2.044422	74.15525	0.045441
26	M_PL_027	17*58	118	0.239351	2.000322	1.331542	33.68995	0.028459
27	M_PL_028	41*139	374	0.131251	4.47164	7.304435	53.32837	0.045958
28	M_PL_029	49*118	346	0.119682	8.91505	3.291805	62.7164	0.039262
29	M_PL_030	23*47	101	0.186864	1.653337	1.62258	32.17102	0.02823
30	M_PL_031	46*45	152	0.14686	4.986067	2.519069	39.71193	0.03188
31	M_PL_032	7*33	65	0.562771	1.196749	4.818948	37.98653	0.029091
32	M_PL_033	14*38	91	0.342105	3.075189	2.500782	41.48556	0.030332
33	M_PL_034	25*126	310	0.196825	5.48773	9.328806	62.07493	0.049749
34	M_PL_035	61*36	178	0.162113	5.920006	3.527713	50.59522	0.033486
35	M_PL_036	10*12	30	0.5	1.098611	1.001852	28.52018	0.030736
36	M_PL_037	10*40	72	0.36	1.665889	2.097024	31.38532	0.029354
37	M_PL_038	8*42	79	0.470238	1.099888	2.218168	31.18603	0.027827
38	M_PL_039	17*51	129	0.297578	4.499766	2.16238	46.06853	0.032645
39	M_PL_040	92*272	567	0.045316	3.879295	5.484114	47.22281	0.072226

Extended Data Fig. 2 | The characteristics of the real networks analysed in the paper. 'ID' is the identity of one network recorded in the website[66]. '|*P*|', '|*A*|' denotes the number of plant and animal species respectively. '|*links*|' is the number of links in a network. '*C*' is the connectivity of a network. 'H_P' and 'H_A' are the heterogeneity of the plant and animal sub-networks respectively. 'γ' is the effective mutual strength. '⟨err⟩' is the prediction error of our method for each network. For data sources and references, see Supplementary **Prediction error**.

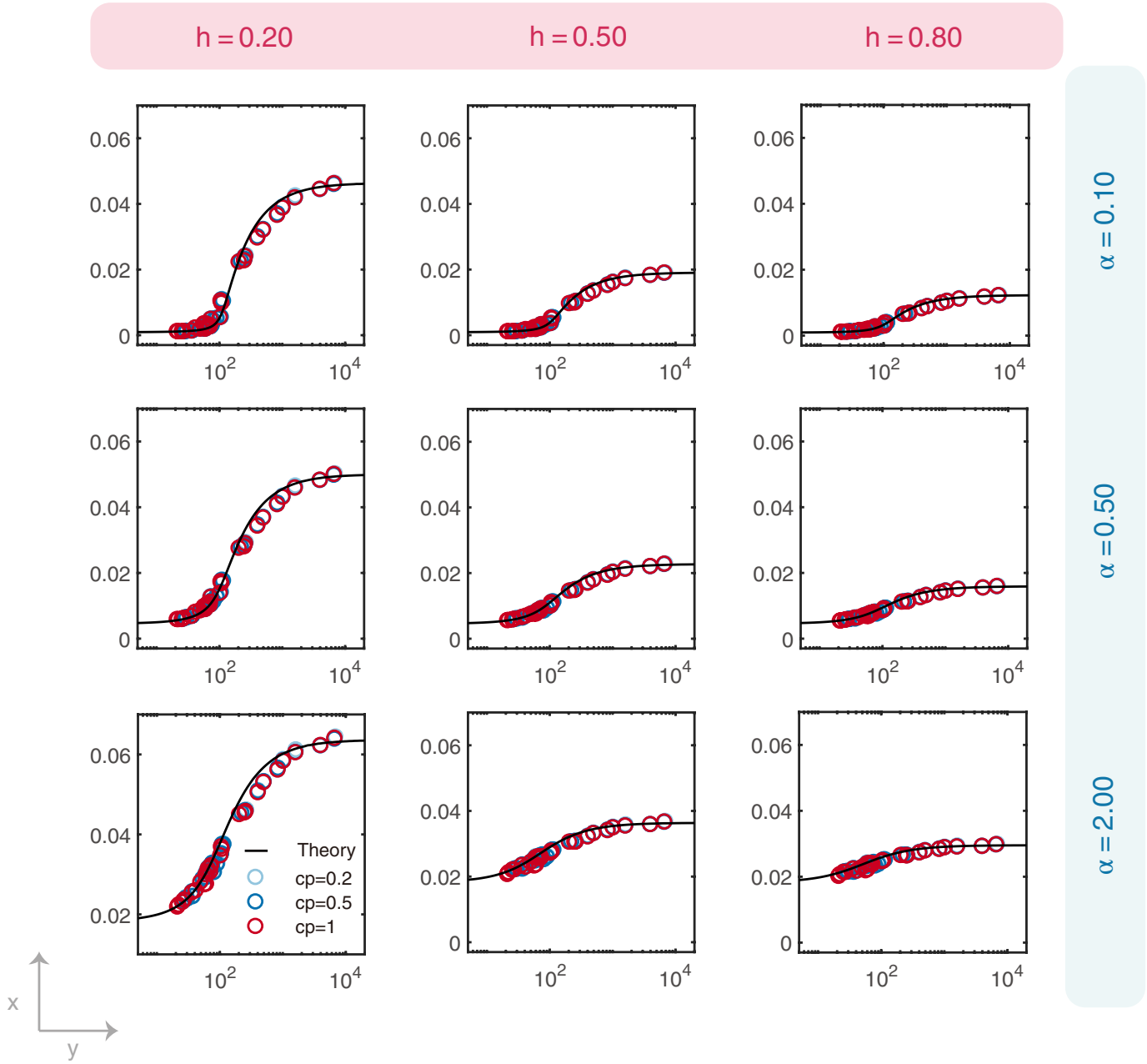

Extended Data Fig. 3 | The robustness of the proposed resilience function for non-transition case. The proposed resilience function (the gray curve, theoretical prediction obtained from equation (1) with $\beta_s = 100$ and $\beta = 10$) predicts well the resilience of 28 weighted networks (see supplementary Table S2) without transition, under different parameters: $\alpha = 2$, $\alpha = 1$, $\alpha = -1$, $h = 0.8$, $h = 0.5$ and $h = 0.2$. Moreover, it is robust to competition typologies by assigning three different linking probabilities: 20% (light blue), 50% (blue), and 100% (red).

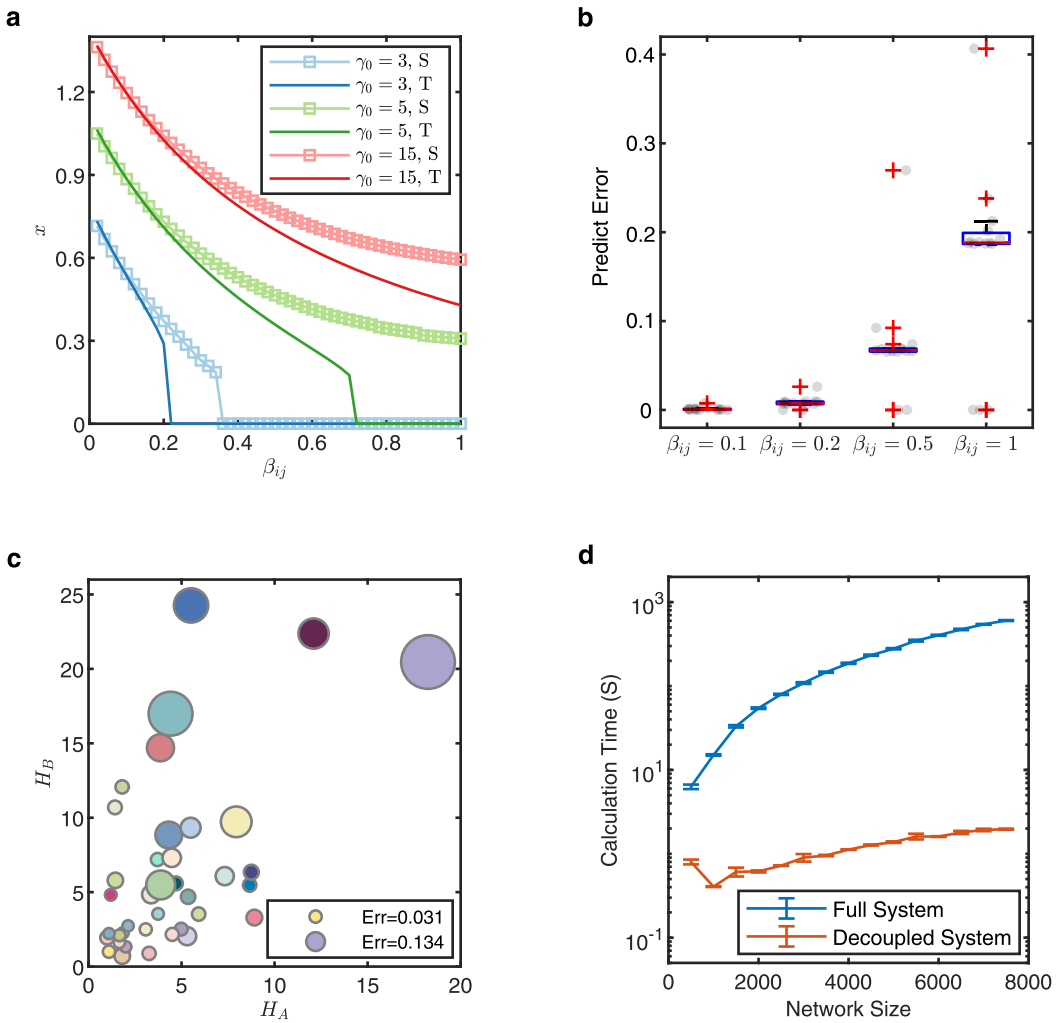

Extended Data Fig. 4 | Prediction fails with large inter-competition strengths and high heterogeneity. a-b, Test how inter-competition strength influence the prediction on a synthetic system with a plants' inter-competition network *A* (a 100*100 ER network), an animals' inter-competition matrix *C* (a 150*150 ER network), and a mutualistic network (a 100*150 ER network), with homogeneous inter-competition β_{ij} and mean degree 5. **a**, The simulation results of the effective abundance for all species ('S', obtained by solving the high-dimensional equations equation (2)) fit well with the theoretical prediction ('T', obtained by numerically solving 1D function $\frac{dx}{dt} = x(\alpha - \beta_w x + \frac{\gamma x}{1+h\gamma x})$ directly) when the inter-specific competition strength β_{ij} is small ($\beta_{ij} < 0.2$ for certain mutual strength $\gamma_0 = [3, 5, 15]$). However, the prediction fails with large inter-competition β_{ij}. **b**, For one γ_0, we calculate the prediction error (difference between 'S' and 'T') for $\beta_{ij} = [0.1, 0.2, 0.5, 1]$ respectively. In each box, there are 15 points ($\gamma_0 = [1{:}15]$). The central mark indicates the median, the bottom and top edges of the box indicate the 25th and 75th percentiles respectively, while the whiskers extend to the most extreme data points not considered outliers (the outliers are marked with '+'). **c**, We show how the heterogeneity of a mutualistic network influences the prediction accuracy applied to 39 real mutualistic networks in Fig. 2q. Firstly, we project each system into two networks[31] and then calculate the heterogeneity of the two networks *that is*, H_P and H_A, respectively. **d**, We compare the calculation time between the full system (equation (1)) and the decoupled system (first solve equation (3) and then put x_{eff} and x_{eco} into equation (4)), for 10 random graphs. Data are presented as mean values +/- SEM. CPU: Single core in Intel(R) Xeon(R) CPU E5-2683 v4 @ 2.10GHz. Parameter setting: $h = 0.2$, $\alpha^{(P)} = -0.3_{N^{\mathrm{I}} \times 1}$, $\alpha^{(A)} = -0.3_{N^{\mathrm{II}} \times 1}$, $\beta_S^{(P)} = \mathrm{diag}(3_{N^{\mathrm{I}} \times 1})$, $\beta_S^{(A)} = \mathrm{diag}(3_{N^{\mathrm{II}} \times 1})$, $\gamma_{ij} = \varepsilon_{ij}\gamma_0/(s_i)^{\delta}$, $\delta = 0.5$.

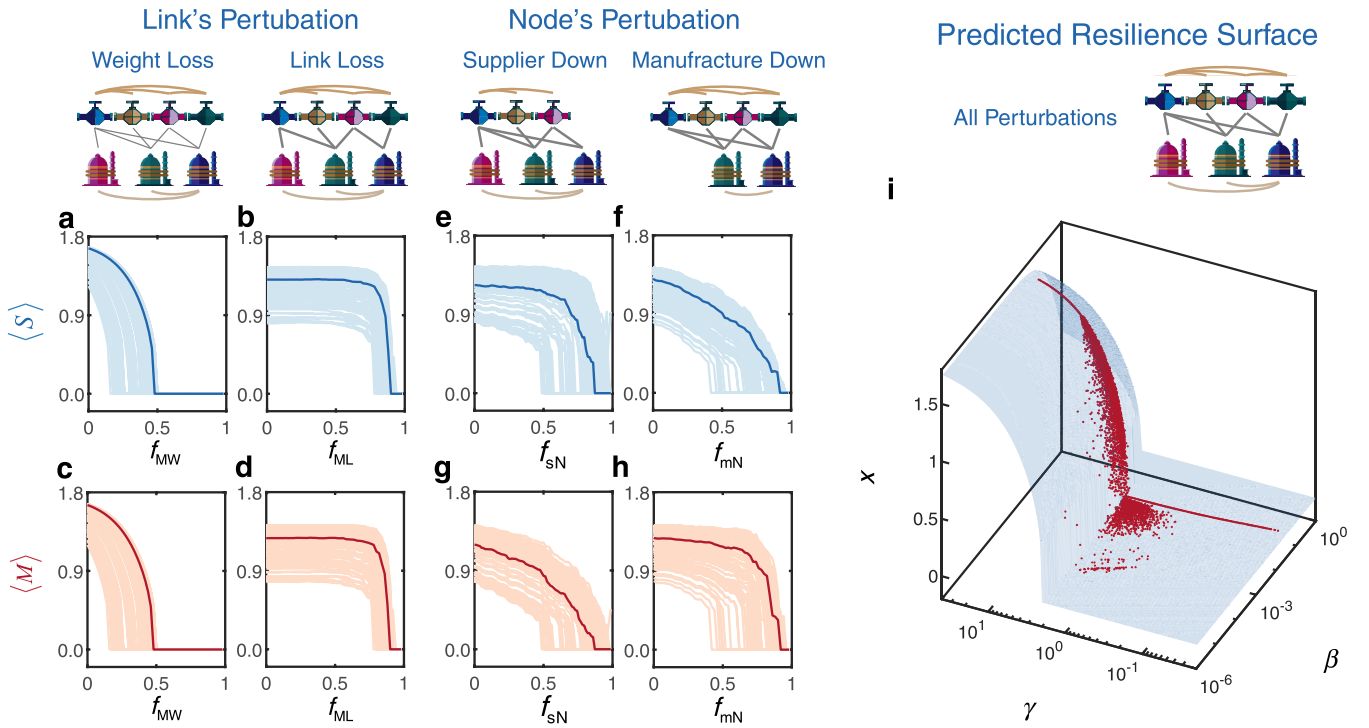

Extended Data Fig. 5 | The prediction of resilience in supply chain networks. The resilience is tested against: (1) perturbation in links (**a**-**d**, for mutualistic network), and (2) perturbation in nodes (**e**-**h**). Link perturbation has two variations: increasing/decreasing (*that is* competition/mutualism) the average weight to a fraction f_w of their original value; and extinction of a fraction f_L of links. Node perturbation also has two variations: extinction of a fraction f_{sN} of suppliers; extinction of a fraction f_{mN} of manufacturers. **i**, All data (red points) in **a**-**h** uniformly collapse onto the resilience function (blue surface), indicating that regardless of the network structures and the forms of perturbation, the state of the system is captured by β and γ (see dynamics for supply chain networks in Supplementary Note 7).

nature portfolio

Corresponding author(s): Jianxi Gao

Last updated by author(s): Jun 30, 2022

Reporting Summary

Nature Portfolio wishes to improve the reproducibility of the work that we publish. This form provides structure for consistency and transparency in reporting. For further information on Nature Portfolio policies, see our Editorial Policies and the Editorial Policy Checklist.

Statistics

For all statistical analyses, confirm that the following items are present in the figure legend, table legend, main text, or Methods section.

n/a	Confirmed	
☐	☒	The exact sample size (*n*) for each experimental group/condition, given as a discrete number and unit of measurement
☐	☒	A statement on whether measurements were taken from distinct samples or whether the same sample was measured repeatedly
☐	☒	The statistical test(s) used AND whether they are one- or two-sided *Only common tests should be described solely by name; describe more complex techniques in the Methods section.*
☒	☐	A description of all covariates tested
☒	☐	A description of any assumptions or corrections, such as tests of normality and adjustment for multiple comparisons
☐	☒	A full description of the statistical parameters including central tendency (e.g. means) or other basic estimates (e.g. regression coefficient) AND variation (e.g. standard deviation) or associated estimates of uncertainty (e.g. confidence intervals)
☐	☒	For null hypothesis testing, the test statistic (e.g. *F*, *t*, *r*) with confidence intervals, effect sizes, degrees of freedom and *P* value noted *Give P values as exact values whenever suitable.*
☒	☐	For Bayesian analysis, information on the choice of priors and Markov chain Monte Carlo settings
☒	☐	For hierarchical and complex designs, identification of the appropriate level for tests and full reporting of outcomes
☐	☒	Estimates of effect sizes (e.g. Cohen's *d*, Pearson's *r*), indicating how they were calculated

Our web collection on statistics for biologists contains articles on many of the points above.

Software and code

Policy information about availability of computer code

Data collection	*Provide a description of all commercial, open source and custom code used to collect the data in this study, specifying the version used OR state that no software was used.*
Data analysis	Matlab

For manuscripts utilizing custom algorithms or software that are central to the research but not yet described in published literature, software must be made available to editors and reviewers. We strongly encourage code deposition in a community repository (e.g. GitHub). See the Nature Portfolio guidelines for submitting code & software for further information.

Data

Policy information about availability of data

All manuscripts must include a data availability statement. This statement should provide the following information, where applicable:

- Accession codes, unique identifiers, or web links for publicly available datasets
- A description of any restrictions on data availability
- For clinical datasets or third party data, please ensure that the statement adheres to our policy

All network and abundance data can be accessed through \url{https://zenodo.org/record/6784072#.Yr3TkOjMKUk} [76].

Human research participants

Policy information about studies involving human research participants and Sex and Gender in Research.

Reporting on sex and gender	*Use the terms sex (biological attribute) and gender (shaped by social and cultural circumstances) carefully in order to avoid confusing both terms. Indicate if findings apply to only one sex or gender; describe whether sex and gender were considered in study design whether sex and/or gender was determined based on self-reporting or assigned and methods used. Provide in the source data disaggregated sex and gender data where this information has been collected, and consent has been obtained for sharing of individual-level data; provide overall numbers in this Reporting Summary. Please state if this information has not been collected. Report sex- and gender-based analyses where performed, justify reasons for lack of sex- and gender-based analysis.*
Population characteristics	*Describe the covariate-relevant population characteristics of the human research participants (e.g. age, genotypic information, past and current diagnosis and treatment categories). If you filled out the behavioural & social sciences study design questions and have nothing to add here, write "See above."*
Recruitment	*Describe how participants were recruited. Outline any potential self-selection bias or other biases that may be present and how these are likely to impact results.*
Ethics oversight	*Identify the organization(s) that approved the study protocol.*

Note that full information on the approval of the study protocol must also be provided in the manuscript.

Field-specific reporting

Please select the one below that is the best fit for your research. If you are not sure, read the appropriate sections before making your selection.

☐ Life sciences ☐ Behavioural & social sciences ☒ Ecological, evolutionary & environmental sciences

For a reference copy of the document with all sections, see nature.com/documents/nr-reporting-summary-flat.pdf

Ecological, evolutionary & environmental sciences study design

All studies must disclose on these points even when the disclosure is negative.

Study description	We use the network structure data and the abundance data to simulate the growth of species in an ecosystem.
Research sample	*Describe the research sample (e.g. a group of tagged Passer domesticus, all Stenocereus thurberi within Organ Pipe Cactus National Monument), and provide a rationale for the sample choice. When relevant, describe the organism taxa, source, sex, age range and any manipulations. State what population the sample is meant to represent when applicable. For studies involving existing datasets, describe the data and its source.*
Sampling strategy	*Note the sampling procedure. Describe the statistical methods that were used to predetermine sample size OR if no sample-size calculation was performed, describe how sample sizes were chosen and provide a rationale for why these sample sizes are sufficient.*
Data collection	Huixin Zhang downloaded the network structure data from the webstie "web of life" (https://www.web-of-life.es/). Huixin Zhang collected the abundance data from 7 previous papers.
Timing and spatial scale	*Indicate the start and stop dates of data collection, noting the frequency and periodicity of sampling and providing a rationale for these choices. If there is a gap between collection periods, state the dates for each sample cohort. Specify the spatial scale from which the data are taken*
Data exclusions	*If no data were excluded from the analyses, state so OR if data were excluded, describe the exclusions and the rationale behind them, indicating whether exclusion criteria were pre-established.*
Reproducibility	*Describe the measures taken to verify the reproducibility of experimental findings. For each experiment, note whether any attempts to repeat the experiment failed OR state that all attempts to repeat the experiment were successful.*
Randomization	*Describe how samples/organisms/participants were allocated into groups. If allocation was not random, describe how covariates were controlled. If this is not relevant to your study, explain why.*
Blinding	*Describe the extent of blinding used during data acquisition and analysis. If blinding was not possible, describe why OR explain why blinding was not relevant to your study.*

Did the study involve field work? ☐ Yes ☒ No

Reporting for specific materials, systems and methods

We require information from authors about some types of materials, experimental systems and methods used in many studies. Here, indicate whether each material, system or method listed is relevant to your study. If you are not sure if a list item applies to your research, read the appropriate section before selecting a response.

Materials & experimental systems

n/a	Involved in the study
☒	☐ Antibodies
☒	☐ Eukaryotic cell lines
☒	☐ Palaeontology and archaeology
☒	☐ Animals and other organisms
☒	☐ Clinical data
☒	☐ Dual use research of concern

Methods

n/a	Involved in the study
☒	☐ ChIP-seq
☒	☐ Flow cytometry
☒	☐ MRI-based neuroimaging